Molecular Cell

Article

The Rab5 effector FERRY links early endosomes with mRNA localization

Graphical abstract

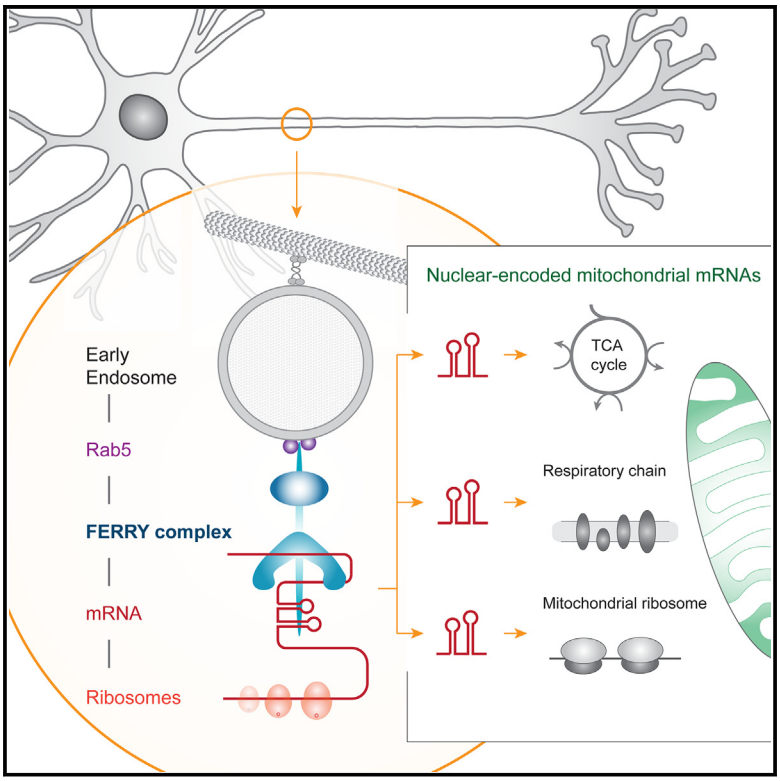

Authors

Jan S. Schuhmacher, Susanne tom Dieck, Savvas Christoforidis, ..., Markus T. Bohnsack, Erin M. Schuman, Marino Zerial

Correspondence

zerial@mpi-cbg.de

In brief

In neurons, efficient and directed mRNA transport into axons and dendrites is necessary to ensure cellular function. Schuhmacher et al. report that the FERRY complex links a subgroup of mRNAs with early endosomes, providing the full logistic capacity of the early endosomal system for mRNA distribution.

Highlights

- Discovery of the Rab5 effector FERRY complex localized to early endosomes
- FERRY binds mRNA selectively, e.g., nuclear-encoded mRNAs for mitochondrial proteins
- The FERRY complex co-localizes with mRNA on early endosomes in neurons
- Loss of FERRY subunits reduces co-localization of mRNAs and early endosomes

Schuhmacher et al., 2023, Molecular Cell *83*, 1839–1855
June 1, 2023
https://doi.org/10.1016/j.molcel.2023.05.012

CellPress

Molecular Cell

CellPress
OPEN ACCESS

Article

The Rab5 effector FERRY links early endosomes with mRNA localization

Jan S. Schuhmacher,[1] Susanne tom Dieck,[2] Savvas Christoforidis,[3,4] Cedric Landerer,[1,5] Jimena Davila Gallesio,[6] Lena Hersemann,[1] Sarah Seifert,[1] Ramona Schäfer,[1] Angelika Giner,[1] Agnes Toth-Petroczy,[1,5] Yannis Kalaidzidis,[1] Katherine E. Bohnsack,[6] Markus T. Bohnsack,[6,7,8] Erin M. Schuman,[2] and Marino Zerial[1,5,9,*]

[1]Max Planck Institute of Molecular Cell Biology and Genetics, Pfotenhauerstrasse 108, 01307 Dresden, Germany
[2]Max Planck Institute for Brain Research, Max-von-Laue-Str. 4, 60438 Frankfurt am Main, Germany
[3]Biomedical Research Institute, Foundation for Research and Technology, 45110 Ioannina, Greece
[4]Laboratory of Biological Chemistry, Department of Medicine, School of Health Sciences, University of Ioannina, 45110 Ioannina, Greece
[5]Center for Systems Biology Dresden, Pfotenhauerstrasse 108, 01307 Dresden, Germany
[6]Department of Molecular Biology, University Medical Center Göttingen, Humboldtallee 23, 37073 Göttingen, Germany
[7]Göttingen Centre for Molecular Biosciences, University of Göttingen, Justus-von-Liebig-Weg 11, 37077 Göttingen, Germany
[8]Max Planck Institute for Multidisciplinary Sciences, Am Fassberg 11, 37077 Göttingen, Germany
[9]Lead contact
*Correspondence: zerial@mpi-cbg.de
https://doi.org/10.1016/j.molcel.2023.05.012

SUMMARY

Localized translation is vital to polarized cells and requires precise and robust distribution of different mRNAs and ribosomes across the cell. However, the underlying molecular mechanisms are poorly understood and important players are lacking. Here, we discovered a Rab5 effector, the five-subunit endosomal Rab5 and RNA/ribosome intermediary (FERRY) complex, that recruits mRNAs and ribosomes to early endosomes through direct mRNA-interaction. FERRY displays preferential binding to certain groups of transcripts, including mRNAs encoding mitochondrial proteins. Deletion of FERRY subunits reduces the endosomal localization of transcripts in cells and has a significant impact on mRNA levels. Clinical studies show that genetic disruption of FERRY causes severe brain damage. We found that, in neurons, FERRY co-localizes with mRNA on early endosomes, and mRNA loaded FERRY-positive endosomes are in close proximity of mitochondria. FERRY thus transforms endosomes into mRNA carriers and plays a key role in regulating mRNA distribution and transport.

INTRODUCTION

Correct subcellular mRNA localization is vital for fundamental biological processes such as embryonic development, cellular homeostasis, neuronal plasticity, and adaptive response to environmental cues.[1–5] For example, asymmetric mRNA localization during oogenesis is required for anterior-posterior patterning of the embryo.[6,7] For neurons, the availability of mRNAs at different subcellular locations is essential due to their unique morphology and function. Axonal and dendritic processes span long distances and confer the ability to respond to external cues on a millisecond timescale far away from the nucleus. The complexity of the task and the transport distances clearly exceed the capacity of diffusion or diffusion-capture mechanisms. Therefore, neurons must either transport or produce proteins at their site of action. Localized translation of protein requires active mRNA transport of the mRNAs encoding them.[8,9] Thus, thousands of different mRNAs are present in axons, dendrites, or the neuropil.[10–12] Furthermore, these transcripts are distributed heterogeneously with mRNAs, showing distinct localization patterns or being exclusive for certain sub-compartments.

Correct subcellular mRNA localization requires a sophisticated molecular regulation tailored to the specific roles of the mRNAs. A direct coupling of RNA-binding proteins (RBPs) and motor proteins has been observed in various forms[13–15] (for example, RBPs recognizing *cis*-regulatory elements on the respective mRNA, including the so called "zipcodes"[5,16]). Recently, several organelles of the endo-lysosomal system have been associated with the spatial organization of mRNAs, messenger ribonucleoprotein (mRNP) granules, and ribosomes in different organisms.[17–19] In the fungus *U. maydis*, a special adaptor system enables the long-distance transport of mRNAs and polysomes on early endosomes (EEs).[17] In higher eukaryotes, lysosomes serve as an Annexin A11-mediated mRNP granule transport vehicle, while late endosomes (LEs) act as translation platforms for mitochondrial proteins in neurons,[18,19] thereby exploiting the full logistic capacity of the endolysosomal system for mRNA distribution.

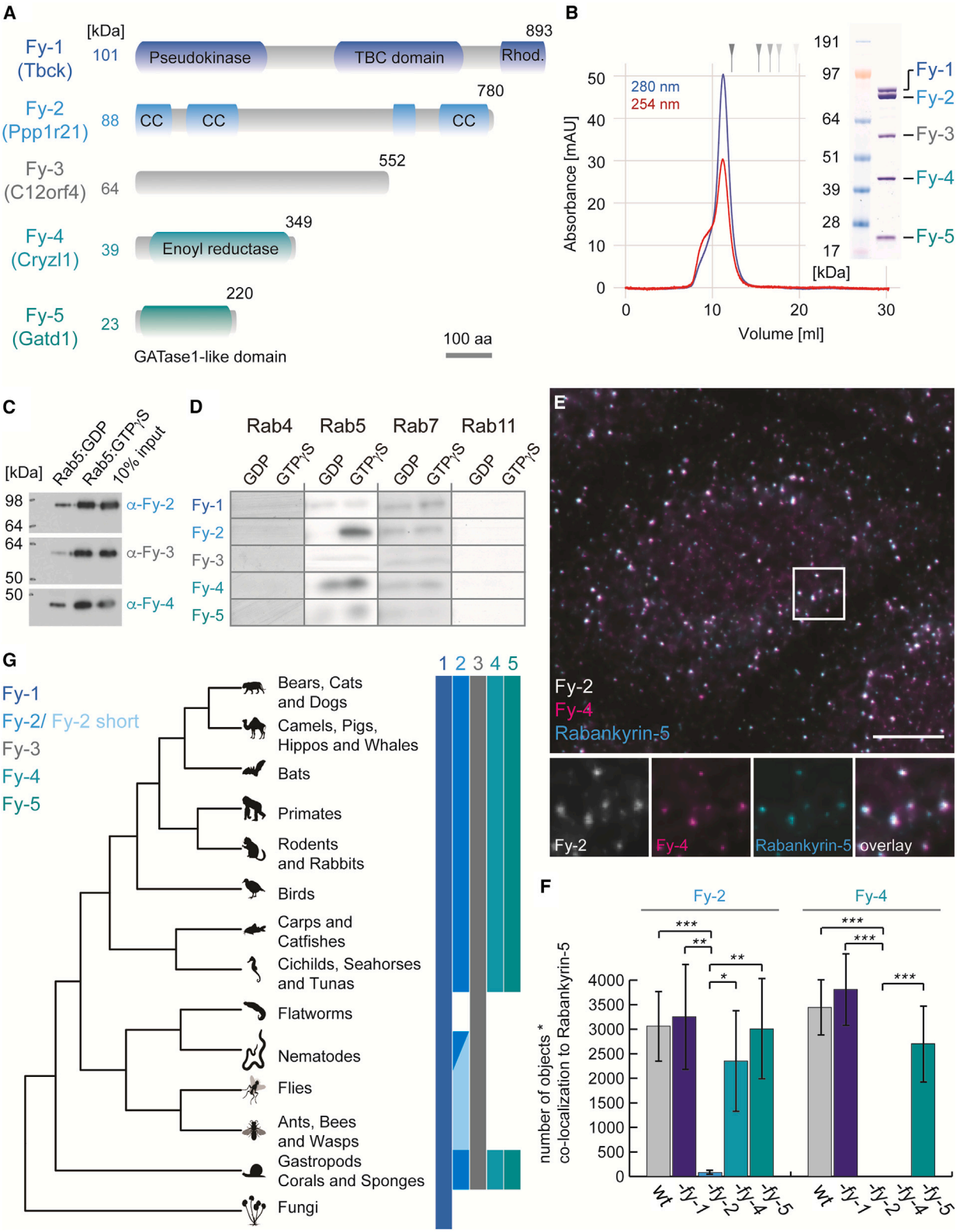

(legend on next page)

Among endocytic organelles, EEs appear particularly suitable to support directional mRNA transport, even more than LEs, due to their bidirectional motility in neurons[20] whereas LEs (multi-vesicular bodies) have a strong bias toward retrograde transport.[21,22] Interestingly, EEs also co-localize with mRNA in HeLa cells.[23] Endosome identity is determined by an intricate interplay between proteins and specific lipids that are intimately linked to Rab guanosine triphosphatases (GTPases).[24,25] Rab4 and Rab11 mark recycling endosomes and Rab7 LEs.[25] Rab5 is the hallmark GTPase of EE, where it recruits a plethora of effectors such as the endosomal tether EEA1[26] or Rabankyrin-5,[27] thereby orchestrating different functions of the organelle.[28–32] To date, the molecular mechanisms describing the connection between EEs and mRNAs remain mysterious. No known mRNA-associated protein localizes on EEs, nor do any endosomal proteins contain known RNA-binding motifs.

Closing this gap, we report the discovery of a five-subunit Rab5 effector complex, which we named five-subunit endosomal Rab5 and RNA/ribosome intermediary (FERRY) complex, which connects EE with mRNA localization through direct interaction with Rab5 and mRNAs.

RESULTS

Identification of the FERRY complex

By purifying Rab5 effectors using affinity chromatography,[26] we observed five proteins co-fractionating in size-exclusion chromatography (SEC) (Figure S1A, left). The same set of proteins co-eluted during anion exchange chromatography (Figure S1A, right), suggesting that they form a complex. Mass spectrometry revealed the identity of the proteins as Tbck (101 kDa), Ppp1r21 (88 kDa), C12orf4 (64 kDa), Cryzl1 (39 kDa), and Gatd1 (23 kDa) (Figure 1A). For clarity, we will refer to this complex as the FERRY complex, with the individual subunits designated Fy-1 to Fy-5 (Figure 1A).

We first reconstituted the FERRY complex *in vitro*. All five subunits eluted as a single peak from SEC (Figure 1B), confirming that they form a stable complex. To estimate the stoichiometry of the components, we compared the intensity of the corresponding signals of a Coomassie-stained SDS PAGE, suggesting a ratio of 1:2:1:2:4 for Fy-1:Fy-2:Fy-3:Fy-4:Fy-5, respectively. Using mass photometry, we obtained a molecular weight of 525 ± 41 kDa for the FERRY complex, nicely fitting the estimated ratios, and a calculated molecular weight of 521 kDa (Figure S1B). This was further corroborated by cryogenic electron microscopy (cryoEM) data showing a ratio of 2:2:4 for Fy-2, Fy-4, and Fy-5.[33] If the FERRY complex is a Rab5 effector, it should predominantly bind to the activated, guanosine triphosphate (GTP)-bound form of Rab5. A pull-down assay and Western blot analysis of different FERRY subunits (Fy-2, Fy-3, Fy-4) revealed a much stronger signal for glutathione S-transferase (GST)-Rab5:GTPγS than GST-Rab5:GDP, confirming that the FERRY complex interacts preferentially with activated Rab5 (Figures 1C and S1D).

We next tested the specificity of FERRY subunits for different endosomal Rab GTPases by probing the binding of *in vitro* translated, ^{35}S-methionine labeled individual components Fy-1-5 to GST-Rab5, -Rab4, -Rab7, and -Rab11 (Figure 1D). Out of the five subunits, only Fy-2 bound to Rab5:GTPγS, but not Rab5:GDP (Figure 1D). In addition, no interaction was observed between the FERRY complex and other Rab GTPases. This indicates that Fy-2 mediates the interaction between the FERRY complex and Rab5:GTP specifically, but none of the endosomal Rab GTPases tested. Hydrogen-deuterium exchange mass spectrometry (HDX-MS) confirmed the interaction and identified the Rab5 binding site near the C terminus of Fy-2.[33] These results indicate that the FERRY complex is indeed a Rab5 effector.

The FERRY complex localizes to EEs

The specific FERRY-Rab5:GTP interaction predicts a localization to EEs. To probe the localization of endogenous FERRY, we could raise antibodies against Fy-2 and Fy-4 suitable for immunofluorescence (Figure S1C). Analysis of Fy-2 and Fy-4 revealed a punctate localization pattern in HeLa cells that resembles the distribution of EEs (Figure 1E). As expected, Fy-2 co-localized very well with Fy-4 (0.85) but also with the early endosomal markers Rabankyrin-5 (0.87) and EEA1 (0.76) (Figure S1E), suggesting that the FERRY complex localizes to EEs.

To confirm that the FERRY complex is recruited to EEs via Fy-2 and explore its functional role, we generated HeLa knockout (KO) cell lines of the FERRY subunits Fy-1, Fy-2, Fy-4, and Fy-5 using CRISPR/Cas9 technology. Loss of the respective protein was confirmed by Western blot analysis (Figure S1F), which also showed that levels of Fy-3 were reduced upon *fy-2* KO (80%) and *fy-1* KO (20%) (Figure S1F). Subsequently, we assessed the localization of Fy-2 and Fy-4 under these conditions by counting the number of fluorescent structures co-localizing with the EE marker Rabenkyrin-5. Fy-2 localization was not significantly changed in any KO lines except upon *fy-2* KO. However, for Fy-4 we observed a complete loss of EE

Figure 1. The FERRY complex is a Rab5 effector complex

(A) Domain architecture of the components of the FERRY complex drawn to scale (scale bar in left lower corner: 100 amino acids [aa]; TBC: Tre-2/Bub2/Cdc16, Rhod.: Rhodanese domain, CC: coiled-coil).

(B) SEC profile of the FERRY complex (blue: 280 nm, red: 254 nm) with a Coomassie-stained sodium dodecyl sulfate polyacrylamide gel electrophoresis (SDS PAGE). Molecular weight standard (670, 158, 44, 17, 1.35 kDa).

(C) Western blot analysis of an *in vitro* pull-down assay of the FERRY complex incubated with glutathione beads with GST-Rab5 loaded with GDP or GTPγS using antibodies against Fy-2, Fy-3, and Fy-4.

(D) Fluorographic analysis of GST binding assays using different Rab GTPases against *in vitro* translated 35S methionine-containing FERRY components.

(E) Immunostaining of HeLa cells against Rabankyrin-5, Fy-2, and Fy-4 (scale bar: 10 μm). A magnification of the boxed region is shown below the image.

(F) Quantification of the fluorescent signal of Fy-2 and Fy-4 in images as in (E). The error bars display the standard error of the mean (SEM). p values are indicated with asterisks (*$p < 0.05$, **$p < 0.01$, ***$p < 0.001$).

(G) Phylogenetic analysis of the subunits of the FERRY complex (complete list of species: Table S1).

co-localization in the *fy-2* and *fy-4* KO cell lines (Figure 1F). This is in agreement with the biochemical (Figure 1D) and structural data[33] showing a Fy-2-mediated FERRY-Rab5 interaction which leads to the recruitment to EEs.

FERRY subunits exhibit a substantial variability in size and domain composition and do not resemble any known endosomal complex (e.g., CORVET/HOPS or ESCRT) (Figure 1A). Tracing the FERRY complex through the course of evolution, we performed a phylogenetic analysis of the FERRY subunits. While Fy-1 is the most ancestral subunit with homologues in some fungi, we also found an assembly of Fy-1, Fy-3, and a short version of Fy-2 in insects and some nematodes. With the evolution of the Chordata, we observed a transition from a three-component assembly to the five-subunit complex via the co-occurrence of two proteins, Fy-4 and Fy-5 and the extension of Fy-2 with the Fy-4 and Fy-5 binding sites (Figure 1G; Table S1). This co-evolution further supports the formation of a complex by the FERRY subunits.

The FERRY complex associates with ribosomes

Disruptive mutations of *tbck* (*fy-1*) or *ppp1r21* (*fy-2*) severely impair brain development and function in human patients, causing symptoms such as a mental retardation, intellectual disability, hypotonia, epilepsy, and dysmorphic facial features resulting in premature death.[34–42] The accumulation of lipofuscin in the human brain further reflects disturbances in the endocytic system,[43,44] suggesting that the FERRY complex carries out an endocytic function essential for brain development and neuronal function.

To gain insights into the cellular role of the FERRY complex, we examined its interaction network using a GST pull-down approach (Figure 2A). We purified a GST-fusion variant of the FERRY complex (GST-FERRY; Figure S2A) and incubated it with HEK 293 cell lysate. Mass spectrometry of the elution fractions revealed 34 potential interaction partners of the FERRY complex (Figure 2B; Table S2). Almost three-quarters of the candidates (73.5%) represent ribosomal proteins of both the large and the small subunit (Figure 2C), suggesting that entire ribosomes may be associated with the FERRY complex.

As ribosomal proteins are frequent contaminants of such assays, we tested the specificity of the ribosome association with FERRY. We generated stably transfected HEK 293 cell lines with inducible expression of Flag-His-Fy-2 or Fy-2-His-Flag. Subsequently, cell lysates were fractionated by sucrose gradient centrifugation, separating the small and the large ribosomal subunits, monosomes, and polysomes from free proteins and RNA (Figure S2B). While the majority of Flag-tagged Fy-2 was found to be non-ribosome-associated, a fraction co-migrated with the different subunits, monosomes, and, to a lesser extent, with polysomes, supporting a FERRY-ribosome association in cells (Figure 2D). This prompted us to test whether and which RNAs accompany these ribosomes. We modified the protocol of the GST-FERRY pull-down to identify transcripts co-eluting with the FERRY complex, which were analyzed by sequencing (Figure 2A). Applying a stringent cutoff (adjusted p value $p_{adj} < 0.01$), we identified 252 mRNAs significantly associated with the FERRY complex (Figure 2E; Table S2). Among these candidates, the largest group (66 transcripts, or 26.2%) constitute nuclear-derived mRNAs encoding mitochondrial proteins. Furthermore, we also identified mRNAs encoding components of the endosomal system and nucleosome (Figure 2F). A gene set enrichment analysis against a gene set collection (MSigDB C5 collection: ontology gene sets) revealed a strong enrichment for mitochondrial matrix genes (#1714), mitochondrial ribosome (#2354), cellular respiration (#480), and tricarboxylic acid (TCA) cycle (#4413) components. In summary, these results suggest that the FERRY complex interacts directly or indirectly with specific groups of mRNAs, especially mRNAs of nuclear-encoded mitochondrial proteins.

The FERRY complex interacts directly and distinctively with specific mRNAs

To test whether FERRY interacts with mRNA directly, we performed electrophoretic mobility shift assays (EMSA). Selected *in vitro* transcribed candidate mRNAs obtained by the previous screen included the 5′ untranslated region (UTR), the open reading frame (ORF), the 3′-UTR, and a short stretch of 50 adenines, yielding a 660-nucleotide, artificially poly-adenylated mRNA for the model gene *mrpl41*. With increasing amounts of *mrpl41* mRNA, an additional higher molecular weight band appeared in the EMSA, indicating that FERRY binds to the mRNA (Figure 3A).

Next, we aimed to validate the FERRY-RNA interaction in cells. We used ultraviolet (UV)-mediated protein-RNA cross-linking, which is a zero-distance cross-linking method that covalently attaches proteins to bound RNAs. We utilized the two HEK 293 cell lines expressing Flag-His-Fy-2 and Fy-2-His-Flag, as the main RNA interface of the FERRY complex is located on Fy-2.[33] After cross-linking, we isolated the Fy-2 tagged proteins by tandem affinity purification under native (anti-Flag) and strongly denaturing (Ni^{2+} affinity) conditions and confirmed their correct size by Western blot (Figure 3B). Furthermore, the isolated material was examined regarding the presence of cross-linked RNA. RNA visualization using ^{32}P labeling revealed a signal at the correct molecular weight for both Fy-2 variants, while the control Flag-His sample was empty (Figure 3B). These results confirm a direct FERRY-RNA interaction mediated by Fy-2 in cells.

To test whether the binding of *mrpl41* mRNA to the FERRY complex is Rab5 dependent, we performed EMSAs with a fixed FERRY/*mrpl41* mRNA ratio and added increasing amounts of Rab5:GTPγS to the assay. This did not have an effect on the FERRY-mRNA interaction, suggesting that Rab5 does not play a role in this process (Figure 3C).

The enrichment of specific subsets of mRNAs in the RNA screen points toward the ability of the FERRY complex to discriminate between different mRNAs. To examine the specificity of mRNA binding, we chose 8 mRNAs out of the 237 candidates that encode proteins fulfilling different mitochondrial functions, such as components of the respiratory chain (*cox6b* and *cox8a*), the ATP synthase (*atp5f1b*), the mitochondrial stress response (*gstp1* and *prdx5*), the mitochondrial ribosome (*mrpl41*), the TCA cycle (*mdh2*), the mitochondrial ubiquitination machinery (*uchl1*), and *pigl* mRNA as negative control and tested their interaction with FERRY using EMSAs. The negative control *pigl* was neither enriched in the GST-FERRY pull-down assay nor significantly changed in the transcriptome analysis of FERRY KO

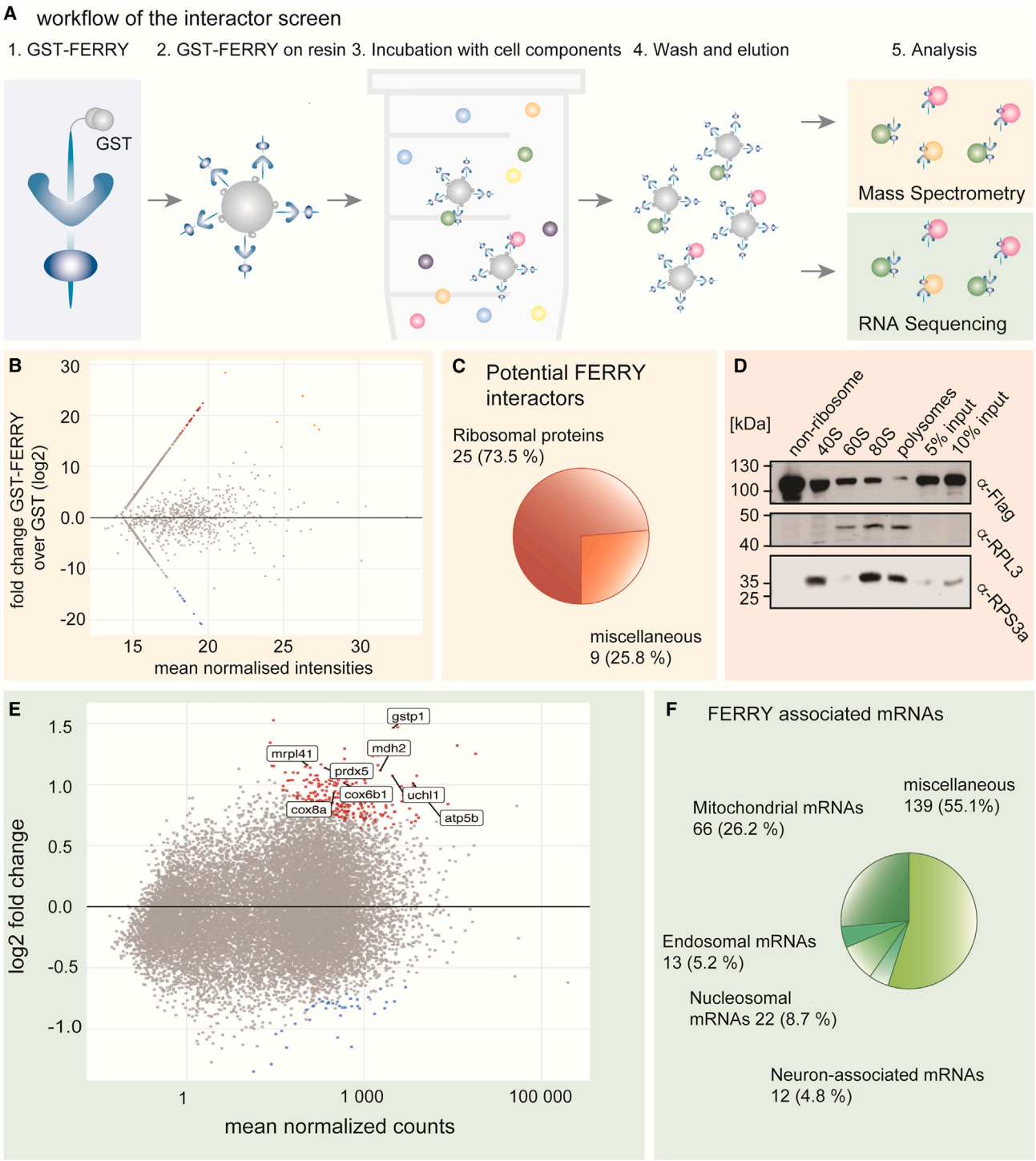

Figure 2. FERRY interacts with ribosomes and associates with a specific subset of mRNAs

(A) Scheme of the *in vitro* GST-FERRY interactor screen.

(B) MA blot of results of the GST-FERRY interactor screen. Candidates enriched in GST-FERRY and GST are indicated in red and blue, respectively.

(C) Pie chart of potential FERRY interactors.

(D) Western blot analysis of sucrose density gradient fractions containing ribosomal (40S, 60S, 80S, and polysomes) and non-ribosomal complexes.

(E) MA blot of the RNA sequencing of potential FERRY-associated mRNAs. mRNA candidates associated with GST-FERRY and GST are highlighted in red and blue, respectively.

(F) Pie chart of the FERRY-associated mRNAs.

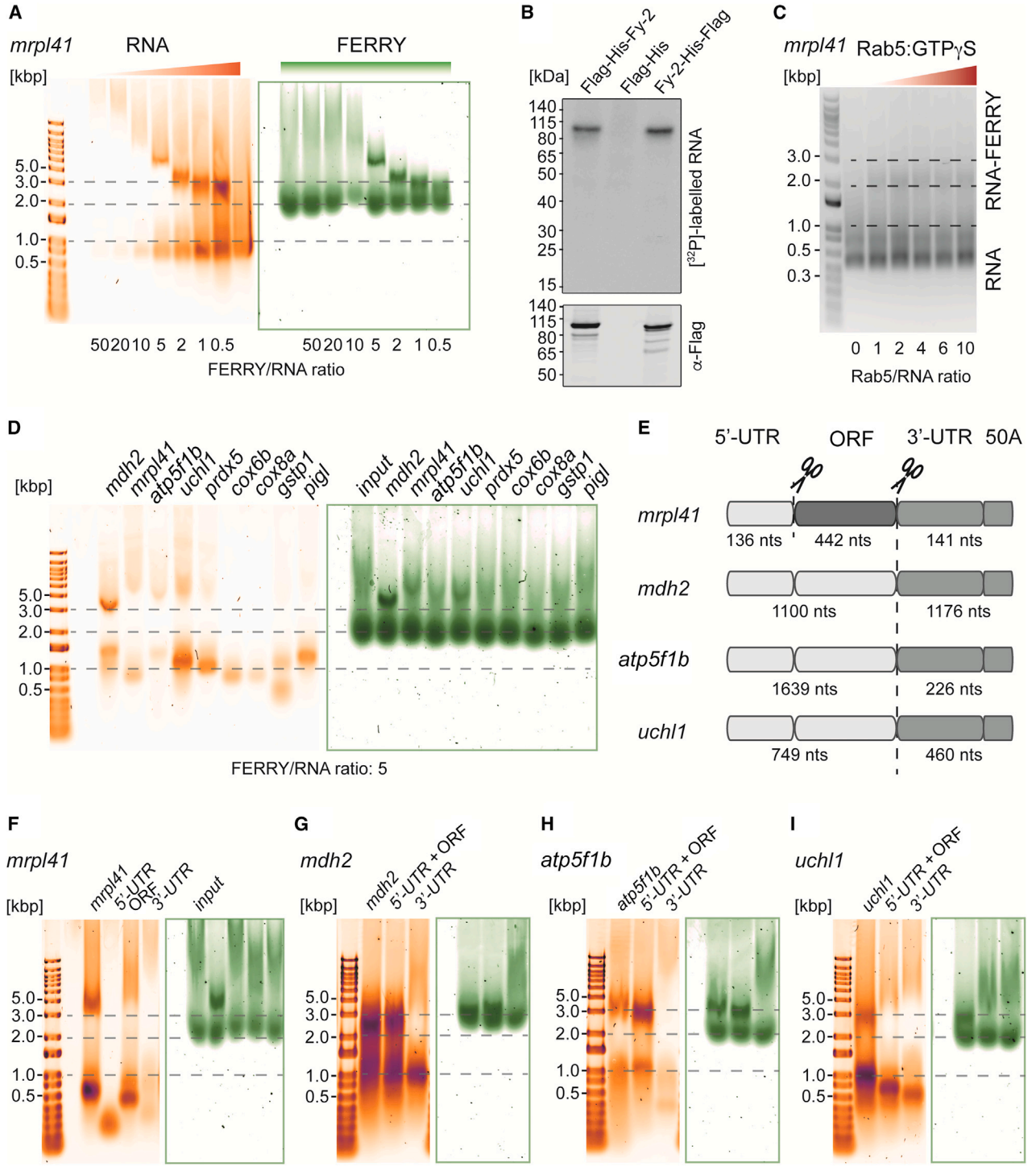

Figure 3. The FERRY-mRNA interaction is selective and involves a complex interface

(A) Electrophoretic mobility shift assay (EMSA) testing the interaction between the FERRY complex (500 nM) and *mrpl41* mRNA by adding increasing amounts of RNA (10 nM–1 μM). (RNA: orange, SYBR Gold; proteins: green, Sypro Red).

(B) Detection of radiolabeled RNAs by autoradiography and Flag-tagged proteins by Western blotting of a tandem affinity purification after UV crosslinking.

(C) EMSAs testing the influence of Rab5:GTPγS (430 nM–4.3 μM) on the interaction of FERRY (430 nM) with mrpl41 mRNA (430 nM). (RNA: gray, ethidium bromide).

(D) EMSAs probing the interaction of FERRY (500 nM) with different mRNAs (100 nM) at a FERRY/RNA ratio of 5.

(E) Scheme of RNA sub-constructs.

(legend continued on next page)

cell lines (see section: The loss of FERRY impacts the cellular transcriptome). While *mdh2*, *mrpl41*, *atp5f1b*, and *uchl1* exhibited interactions with the FERRY complex, the interaction with the other five candidates was much weaker (Figures 3D and S3A). These results suggest that the FERRY complex selectively binds transcripts *in vitro*.

To determine whether the FERRY complex binds different classes of RNA in general, we tested its ability to interact with small RNAs (<200 nts) and different tRNAs ($tRNA^{Arg(ACG)}$, $tRNA^{Cys(GCA)}$ and $tRNA^{Phe(GAA)}$)[45] using EMSA assays. Even at equimolar FERRY-to-RNA ratios, we were unable to detect any interaction, indicating a preference of FERRY for mRNAs (Figures S3B–S3D).

The interaction of the FERRY complex with mRNAs (600–2,200 nucleotides [nts]) raises the question about the binding interface on the mRNA. To determine the location of the interface, we divided four mRNAs (*mrpl41*, *mdh2*, *atp5b*, and *uchl1*), all of which are capable of binding to the FERRY complex (Figure 3D), into different parts (Figure 3E). *mrpl41* mRNA was split into 5′-UTR, ORF, and 3′-UTR with an addition of 50 adenine nts. While the two UTR fragments did not show any interaction with the FERRY complex, the ORF fragment retained the ability to bind FERRY, albeit weaklier than full-length *mrpl41* mRNA (Figures 3F and S3E). The other three candidates were divided into two parts, the 5′-UTR + ORF and the 3′-UTR with 50 adenines. The *mdh2*-FERRY and *atp5b*-FERRY interactions were clearly mediated by the 5′-UTR + ORF fragments, while the 3′-UTR +50A fragments did not bind the FERRY complex (Figures 3G, 3H, S3F, and S3G). Interestingly, for *uchl1* mRNA, both parts still interacted with the FERRY complex, albeit showing reduced binding (Figures 3I and S3H). Altogether, these results argue against two things: first, an unspecific FERRY-mRNA interaction and, second, an interaction mediated by a single, short motif on the mRNAs. They point toward a more complex regulation that confers preference of FERRY for certain mRNAs. This is supported by the structural analysis which showed a large interface involving different subunits of the FERRY complex with mRNA.[33]

The FERRY complex impacts mRNA localization in HeLa cells

To investigate the cellular role of the FERRY-mRNA interaction, we compared the localization of different mRNAs to EEs (labeled by EEA1) upon loss of FERRY subunits (Figure 4A). To visualize mRNA more generally, we also included a probe against *polyA*. The candidate set was chosen to include mRNAs binding to the FERRY complex *in vitro* (i.e., *mdh2*, *mrpl41*, and *atp5f1b*), mRNAs identified in our RNA association screen but unable to bind *in vitro* (*cox8a*, *cox6b*, and *gstp1*), and mRNAs that were inconspicuous in both experiments (*mrps35*, *rims1*, *psma1*, and *gla*). We used automated confocal microscopy to acquire large datasets allowing for quantitative image analysis and reliable statistics.

The *polyA* probe yielded a very dense fluorescent signal, as expected for staining the bulk of fully processed mRNA (Figure 4B). Several EEs co-localized or were proximal to *polyA*. However, given the high density of both EEs and *polyA* signals signal overlaps by random co-localization must be ruled out. Therefore, we specifically quantified the mRNA signal associated with EEs by correcting for random co-localization during image analysis. We estimated 9.4% co-localization between *polyA* and EEA1-positive EEs in wild-type (wt) cells, which was reduced in the FERRY subunit KO cell lines, ranging from 6.7% to 5.6% (Figures 4B and 4C, left). For proper quantification and better visualization, we normalized the *polyA*-EE co-localization of the KO cell lines to wt. All four FERRY subunit KO cell lines exhibited a significant decrease in *polyA*-EE co-localization. The KO of *fy-1* had the strongest effect, with the frequency of mRNA-EE co-localization reduced by 43%. Also, the other KO cell lines showed a reduction of EE mRNA co-localization by 35%, 31%, and 30% for the *fy-2*, *fy-4*, and *fy-5* KO, respectively (Figure 4C, right). The reduction by a third or more of mRNA load of EEs in the absence of FERRY subunits suggests that the FERRY complex contributes significantly to the recruitment of mRNA on EEs in addition to other RBPs.[46]

To ensure that the mRNA co-localization to EE is specific, we visualized the FERRY complex, the EE, and the mRNA concomitantly by multicolor super-resolution microscopy. With multiple signal classification (MUSICAL), we acquired up to four different components and reached a resolution of 60 nm for mRNA and 100 nm for endosomal markers (see STAR Methods). Firstly, we combined the staining for Fy-2, EEA1, and *polyA* and observed co-localization and/or partial co-localization with the fluorescence signals in very close proximity (<200 nm) (Figure 4D). The enhanced resolution allowed for the resolving of the fluorescent signals and the detection of instances where Fy-2 appeared to bridge EEA1 and the mRNA (Figure 4D, box). Given the sizes of EEA1 (extended conformation >200 nm), Fy-2[33], and mRNA (Figure S4A), one cannot expect an absolute co-localization. The observed distances are within the expected range of a FERRY-mediated attachment of mRNA to EEs (Figure S4A). Secondly, we used both available FERRY markers (Fy-2 and Fy-4) in combination with Rabankyrin-5 (EE marker) and mRNA (*polyA*). We often observed mRNA, FERRY, and EE partially co-localizing within a range of 250 nm and events where FERRY and the EE co-localized while the signal for the mRNA was slightly shifted (Figure 4E). Again, we detected events where both FERRY markers were located between EE and mRNA (Figure 4E, box). These data validate the co-localization of FERRY-mRNA interaction by confocal microscopy (Figures 4A–4C) and corroborate the notion that the FERRY complex connects the EE with mRNA.

Next, we examined the localization of individual mRNAs to EE upon deletion of FERRY subunits. While the *polyA* probe provided a very dense mRNA staining, the probes against individual mRNAs (Figure 4B) yielded a scarce fluorescent signal with a

(F) EMSAs comparing the FERRY (500 nM)/ RNA (250 nM) interaction of *mrpl41* with its sub-constructs shown in (E).
(G) EMSAs comparing the FERRY (500 nM)/ RNA (250 nM) interaction of *mdh2* with its sub-constructs shown in (E).
(H) EMSAs comparing the FERRY (500 nM)/ RNA (250 nM) interaction of *atp5f1b* with its sub-constructs shown in (E).
(I) EMSAs comparing the FERRY (500 nM)/ RNA (250 nM) interaction of *uchl1* with its sub-constructs shown in (E).

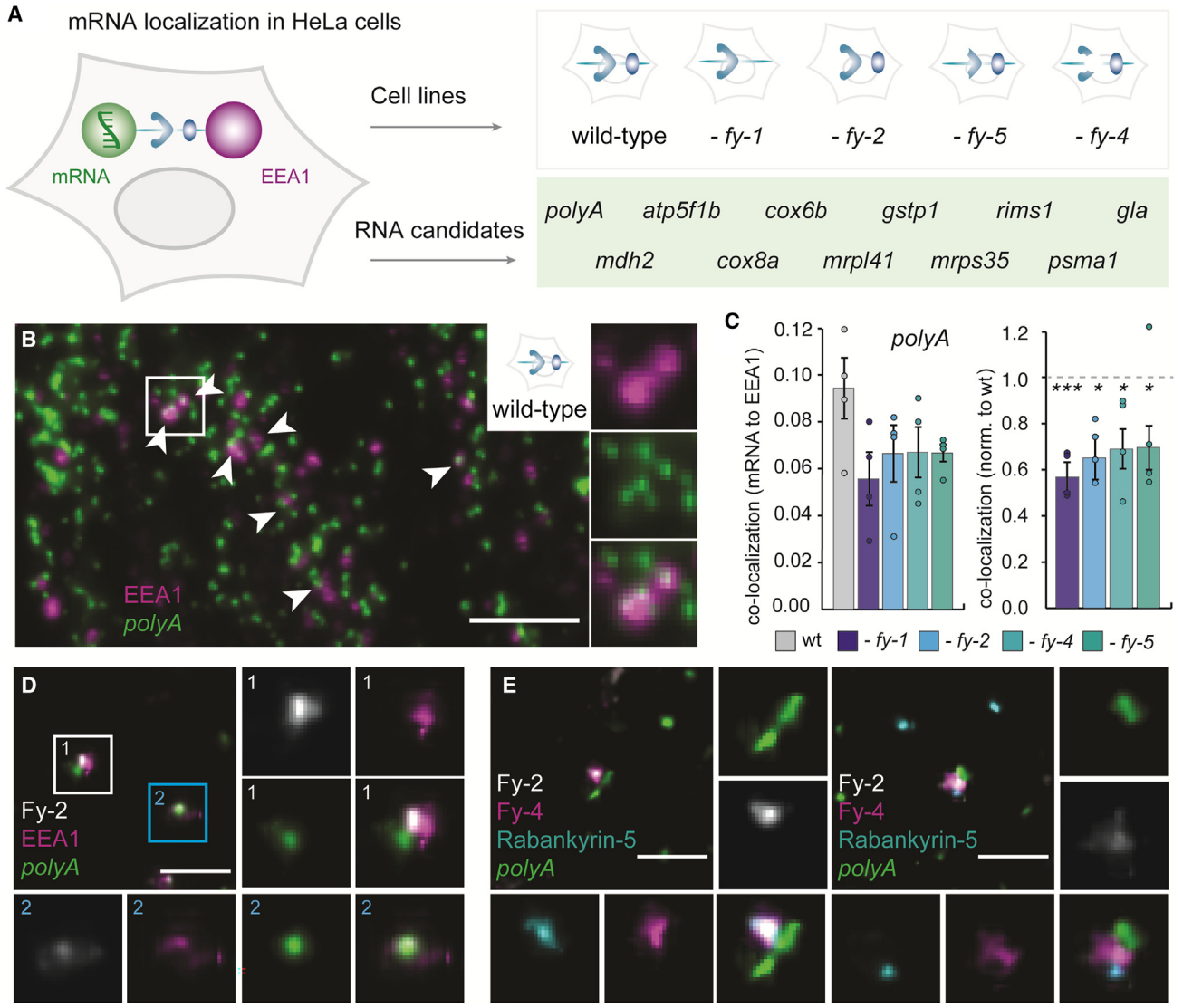

Figure 4. Deletion of FERRY subunits reduces mRNA recruitment to EEs

(A) Scheme of the localization experiment, showing different markers (mRNA: single-molecule fluorescence *in situ* hybridization (smFISH), EEA1: antibody), mRNAs (in the green box), and cell lines (gray box).

(B) Visualization of EEA1 and *polyA* in wt HeLa cells (Scale bar: 5 μm). Co-localization events are indicated with white arrowheads, and the boxed region is highlighted on the right.

(C) Co-localization of *polyA* and EEA1 in HeLa wt and different KO cell lines. The bar graphs show the fraction of co-localizing mRNA (left) and the results normalized to wt (right). The results of the individual biological replicates are indicated by dots, and the error bars display SEM. p values (*fy* KO compared to wt) are indicated with asterisks (*p < 0.05, **p < 0.01, ***p < 0.001).

(D) Super-resolution (MUSICAL) imaging with indicated markers (Scale bar: 1 μm). boxed regions are magnified.

(E) Super-resolution (MUSICAL) imaging with indicated markers (Scale bar: 1 μm).

small number of foci per cell as seen for *atp5f1b* (Figure 5A). Though challenging, we obtained good statistics for this experiment by acquiring large datasets.

We analyzed the co-localization of individual mRNAs with EEs and observed a range of co-localization (11.6%–20.4%) in wt cells (Figure S4B). Again, such co-localization decreased upon FERRY subunit KO for certain mRNAs. For example, the co-localization of *atp5f1b* mRNA with EEs decreased in all four FERRY KO cell lines to a similar extent from 16% to around 10% (Figures 5A and 5B, left), indicating an average reduction of 35% *atp5f1b* mRNA on EEs (Figure 5B, right). In general, the loss of Fy-1 had the strongest impact on mRNA localization. All mRNA probes except *gstp1* showed a significant decrease in EE co-localization in the *fy-1* KO cell line. This observation coincides with Fy-1 being the most conserved subunit of the complex (Figure 1G). The loss of either Fy-2 or Fy-4 reduced EE localization of several mRNAs: *atp5f1b*, *mdh2*, *cox6b*, and *mrps35* mRNAs in the case of *fy-2* KO, and *atp5f1b*, *mdh2*, and *gla* mRNAs in the case of *fy-4* KO.

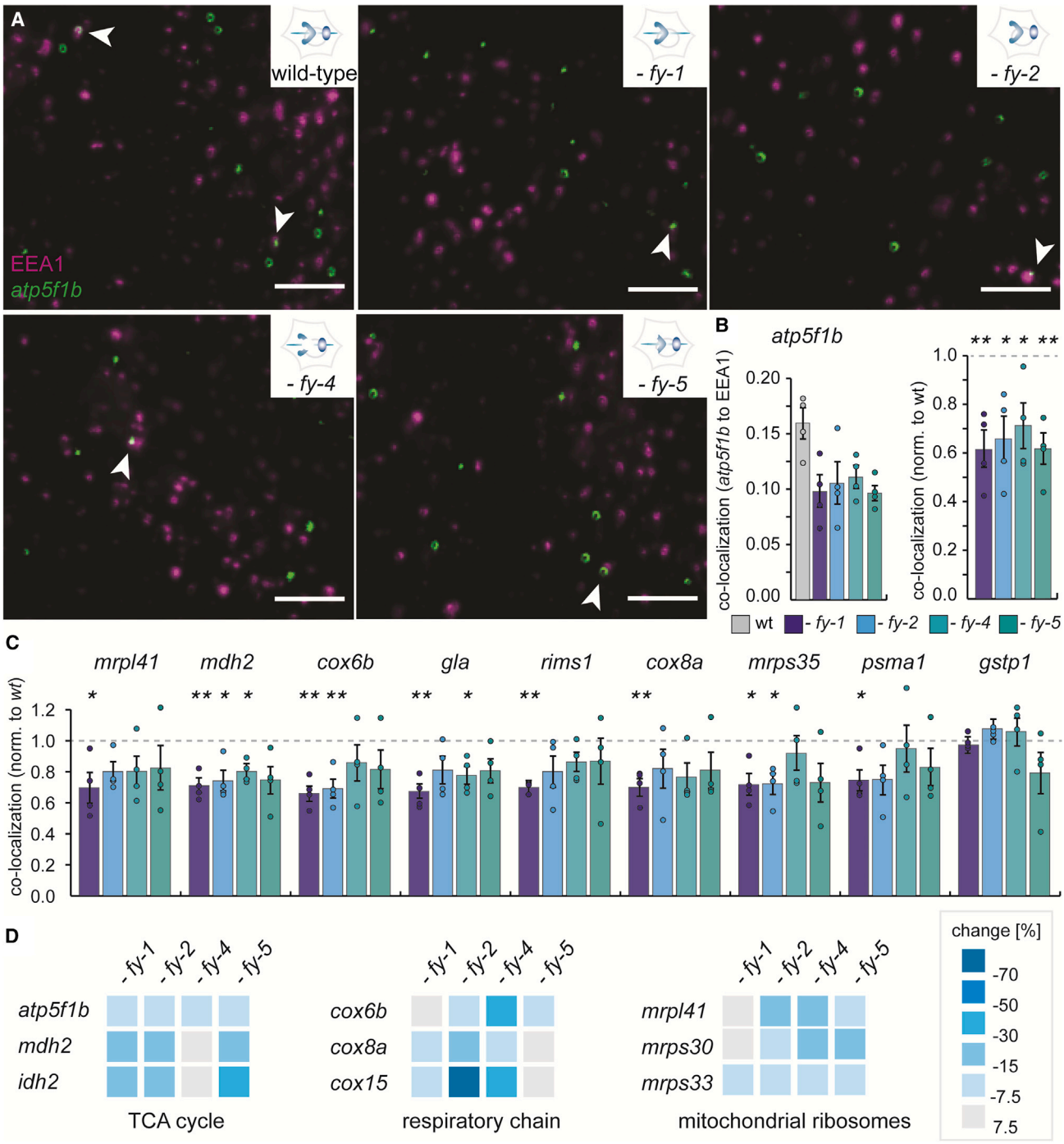

Figure 5. Specific mRNA levels and their recruitment to EEs are decreased upon FERRY subunit deletion

(A) Representative images of EEA1 and *atp5f1b* mRNA in HeLa wt and different KO cell lines. White arrowheads indicate co-localization events. (Scale bar: 5 μm).

(B) Co-localization of *atp5f1b* mRNA and EEA1 in HeLa wt and different KO cell lines. The bar graphs show the fraction of co-localizing mRNA (left) and the results normalized to wt (right). The results of the biological replicates are indicated by dots and the error bars display the SEM. p values (*fy* KO compared to wt) are indicated with asterisks (*p < 0.05, **p < 0.01, ***p < 0.001).

(C) Normalized co-localization of EEA1 and different mRNAs in the FERRY subunit KO cell lines. The results of the biological replicates are indicated dots and the error bars display the SEM. p values (*fy* KO compared to wt) are indicated with asterisks (*p < 0.05, **p < 0.01, ***p < 0.001).

(D) Changes in mRNA levels of specific genes are given in percent compared to wt.

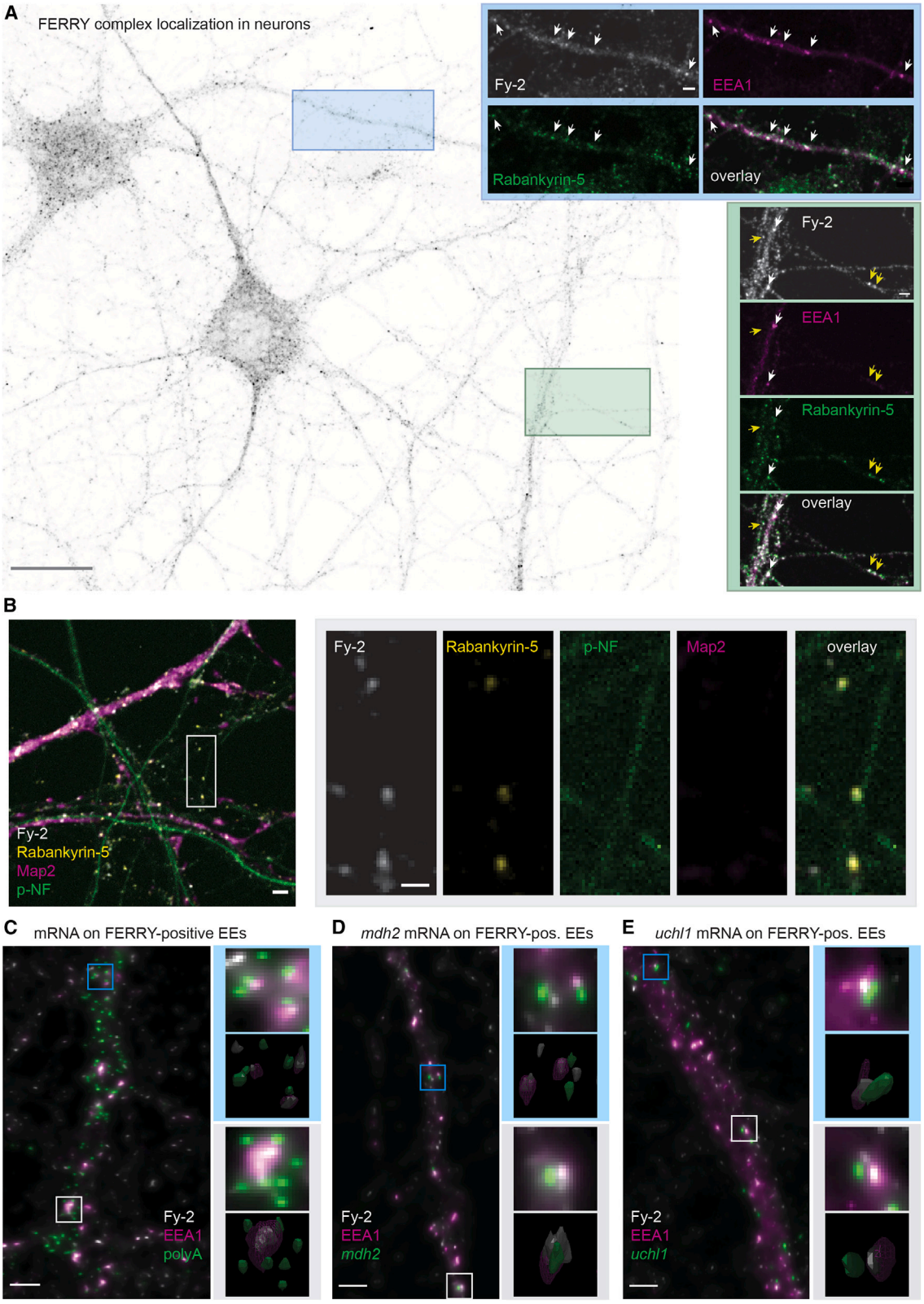

(legend on next page)

In the absence of the smallest subunit Fy-5, only *atp5f1b* mRNA was affected (Figure 5C). The results of the *fy-5* KO suggest that without Fy-5, the FERRY complex is partially functional and the binding to certain mRNAs unaltered. This can be explained by the structure of the FERRY complex, which revealed that Fy-5 contributes a small part to a larger interface and, thus, its loss has only a minor impact on mRNA binding.[33] These data suggest that the FERRY complex plays a major role in mRNA recruitment to EEs. The observation that some mRNAs are more affected than others underlines the notion that the FERRY complex exhibits binding selectivity for mRNAs.

The loss of FERRY impacts the cellular transcriptome

Next, we investigated the influence of a loss of FERRY subunits on mRNA levels. By analyzing the transcriptome of the FERRY subunits KO cell lines, we observed a wide range of changes in mRNA levels (Figure S5A). Given the complexity of alterations, we focused on the changes shared by the loss of all FERRY subunits, or specifically in the *fy-1* and *fy-2* KO cell lines (Figure S5B). Interestingly, although the upregulated mRNAs were spread among a large number of cellular processes, the downregulated mRNAs were focused on fewer pathways connected to nucleosomes, DNA packaging, and nuclear-derived mitochondrial mRNAs, including mRNAs encoding proteins of the TCA cycle, the respiratory chain, and mitochondrial ribosomes. The levels of mRNAs that exhibited a FERRY-dependent recruitment to EEs and related genes were moderately to strongly (between 8% and 78%) downregulated in at least three of the four KO cell lines (Figure 5D). Interestingly, these include *mdh2* and *atp5f1b*, which were shown to bind to FERRY *in vitro* (Figures 3G and 3H), suggesting that FERRY binding and/or localization to endosomes stabilizes these transcripts. However, the observed downregulation of mRNAs did not significantly affect the Mdh2 and Mrpl41 protein levels (Figure S5C), as this usually requires stronger changes in mRNA levels. We cannot exclude effects on localized translation which may be compensated for by the diffusion of mRNAs and proteins in cells with compact morphology, such as HeLa cells, but become detrimental in neurons given their long processes.

In summary, the loss of FERRY subunits caused a moderate downregulation of nuclear-encoded mRNAs for mitochondrial proteins, which might be explained by mis-localization of the respective mRNAs.

The FERRY complex localizes to both the somatodendritic region and axons

Since mutations in FERRY subunits impair brain development and function, we assessed the intracellular localization of the FERRY complex in primary rat hippocampal neurons. We compared the FERRY localization with respect to EEA1 and Rabankyrin-5. In neurons, EEA1 is restricted to the somatodendritic region,[47] whereas Rabankyrin-5 is also found in axons.[20] Again, we observed a punctate pattern of fluorescent foci dispersed across the neuron for Fy-2 (Figure 6A, overview), and the fluorescent signal strongly co-localized with the endosomal markers EEA1 and Rabankyrin-5. We observed many triple positive (Fy-2, EEA1, Rabankyrin-5) endosomes (Figure 6A, details, white arrowheads) but also fluorescent foci that were only positive for Fy-2 and Rabankyrin-5, mainly in thin structures devoid of EEA1 (Figure 6A, yellow arrowheads). These results suggest that the FERRY complex is present in both the somatodendritic region and axons.

To validate this finding, we performed immunofluorescence against Map2 and the phosphorylated neurofilament (pNF)-1 as markers of the somatodendritic region and axons, respectively (Figure 6B, overview). We observed Fy-2- and Rabankyrin-5-positive EEs in thin structures positive for the axonal marker pNF (Figure 6B, box). In summary, the FERRY complex resides on EEs distributed across the neuronal soma, dendrites, and axons, raising the question about possible mRNA localization on these endosomes.

The FERRY complex co-localizes with mRNA on EEs in neurons

To investigate whether FERRY-positive EEs also carry mRNA in neurons, we visualized the majority of mRNAs using a *polyA* probe and focused on imaging dendrites and axons since the cell body has a high signal density. While the mRNA density in major dendrites is still high, it decreases in thinner processes and forms clusters at nodes. Overall, we observed 6.1% of mRNA foci co-localizing with the FERRY complex (Figure 6C). Often, these structures also co-localized with EEA1, suggesting that a fraction of mRNAs are located on EEs (Figure 6C, light blue box). Interestingly, we detected the presence of a larger endosome surrounded by several mRNA foci, with the fluorescent signals in close proximity rather than co-localizing (Figure 6C, white box). This suggests that multiple mRNAs can be attached to large-sized endosomes. Deconvolution allowed us to attain a lateral resolution of ~150 nm (x, y coordinates), while the z-resolution of confocal microscopy is > 500nm. Hence, only partial co-localization will be observed for fluorescent signals in close proximity even within a distance of 250 nm, which is the expected range of a FERRY-mediated attachment of mRNA to the EE (Figure S4B). In case of dense fluorescent signals, similar to those of *polyA*, a substantial proportion of apparent co-localization might result from random co-localization. Therefore, we estimated the random co-localization[48] (Figure S6A, left). The

Figure 6. FERRY co-localizes with EEs and mRNA in neurons

(A) Localization of the FERRY complex in neurons. Overview image: (scale bar: 20 μm). The boxed regions (blue and green) are highlighted and shown with additional markers (EEA1, Rabankyrin-5) (scale bar: 2 μm). White arrowheads indicate co-localization of Fy-2, EEA1, and Rabankyrin-5; yellow arrowheads indicate co-localization of Fy-2 and Rabankyrin-5.

(B) Primary rat hippocampal neurons were stained for Fy-2, Rabankyrin-5, Map2, and a phosphorylated neurofilament (pNF) (scale bar: 2 μm). The boxed region is highlighted on the right (scale bar: 1 μm).

(C)-E) Hippocampal neurons stained for Fy-2, EEA1 and *polyA,* or *mdh2* or *uchl1*. Magnifications and a 3D representation of the indicated regions (gray, blue) are given on the right. (Scale bar: 2 μm).

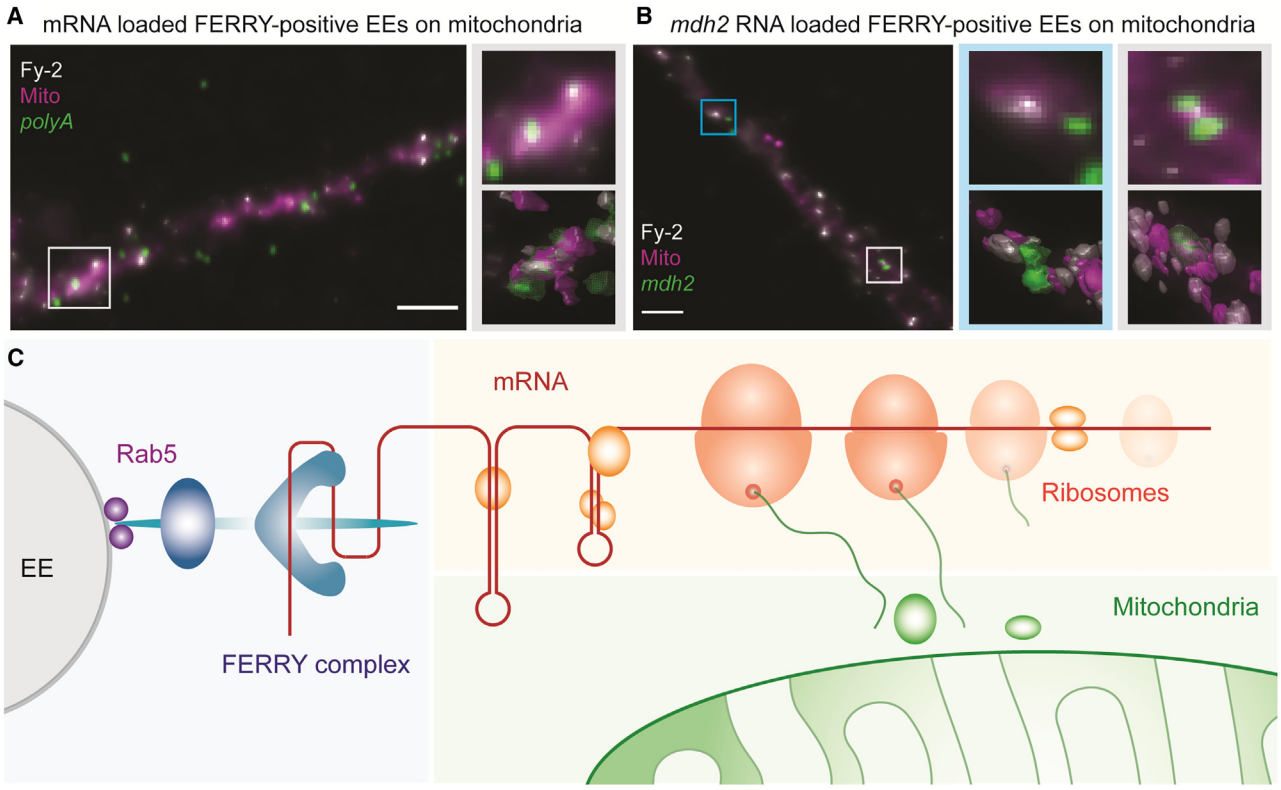

Figure 7. FERRY co-localizes with mRNA encoding for mitochondrial proteins and mitochondria

(A and B) Hippocampal neurons stained for Fy-2, TOM70 and *polyA,* or *mdh2*. Magnifications and a three-dimensional (3D) representation of the indicated regions (gray, blue) are given on the right. (Scale bar: 2 μm).

(C) Scheme of the cellular role of the FERRY complex.

analysis indicated that the co-localization of Fy-2 and mRNA is significantly higher than random chance, supporting the interpretation that mRNAs are associated with EEs (Figure S6A, right).

We next tested the co-localization of the FERRY complex with specific transcripts in neurons, focusing on the *mdh2* and *uchl1* mRNAs based on the initial mRNA-binding screen (Figure 2E) and the co-localization experiments in HeLa cells (Figure 4E). Visualizing individual mRNAs, we obtained much less fluorescent signal per cell (Figures 6D and 6E). Nevertheless, we observed fluorescent signals partially overlapping or in close proximity below 250 nm with the FERRY complex (Figures 6D and 6E boxes), quantified as 13.2% of *mdh2* and 10.3% of *uchl1* mRNAs.

mRNA-loaded FERRY-positive endosomes co-localize with mitochondria

The interaction between the FERRY complex and transcripts encoding mitochondrial proteins suggests that FERRY-positive EEs loaded with mRNAs might be observed in the proximity to mitochondria for localized translation. To examine this, we additionally stained neurons with TOM70 as a marker for mitochondria. When visualizing the *polyA* mRNA population, we found co-localization of the FERRY complex with mRNA on mitochondria (Figure 7A). We also assessed the co-localization of the FERRY complex with the *mdh2* mRNA and mitochondria (Figure 7B). Even though these events were infrequent, we observed examples where the fluorescence signal of the FERRY complex, the *mdh2* mRNA, and mitochondria were in close proximity (Figure 7B, blue box) or even co-localizing (Figure 7B, gray box). Despite the abundance of mitochondria, the degree of co-localization of mRNAs, FERRY, and mitochondria was above the expected value for random co-localization, indicating the detection of biologically meaningful events (Figure S6B). This supports the notion that the FERRY complex is involved in the localization and the distribution of specific mRNAs such as transcripts encoding mitochondrial proteins (e.g., *mdh2* mRNA), most likely by mediating their endosomal transport (Figure 7C).

DISCUSSION

The discovery that both mRNAs and ribosomes can be transported long-range intracellularly by endosomal carriers[17–19] has uncovered new mechanisms underlying spatially controlled mRNA localization and protein translation. Understanding these mechanisms requires elucidating the precise identity of both endosomal carriers and molecular factors binding the mRNAs on these compartments. Here, we discovered the Rab5 effector complex FERRY composed of five subunits, Fy-1 to Fy-5, which interacts with activated Rab5, localizes to EEs, and directly interacts with and recruits mRNAs onto EEs, enabling the cell to

exploit the full logistic capacity of the endosomal system to organize mRNA transport and distribution (Figure 7C).

mRNA binding of the FERRY complex

The FERRY complex differs from previous RBPs and displays a complex RNA-binding mode. It does not contain known RNA-binding domains, and at least three subunits engage in mRNA binding. Also, the involvement of a coiled-coil structure in the mRNA interface has not been observed before. Moreover, we could not pinpoint clear interaction motifs on the RNA. These observations suggest that the FERRY complex constitutes a yet uncharacterized class of RBPs. Despite the large RNA-binding interface on the FERRY complex, we only detected moderate binding affinities to mRNAs *in vitro*. This points toward additional layers of regulation *in vivo*, which might include post-translational modifications, structural features, or additional factors. Given the number of mRNAs that are produced in the cell, an elaborate regulation of mRNA binding seems more likely than a simple affinity-driven FERRY-mRNA interaction. Taken together, the FERRY complex exhibits unusual RNA-binding features and offers the possibility to gain deeper insights in RNA-protein interactions.

mRNA transport on endosomes

The coupling between the endosomal system and mRNA[18,19,23] raises the question as to which transcripts bind to endosomes, how many mRNA binding-sites endosomes can offer, and whether these are provided by different RBPs. We could visualize several—up to four—mRNA foci associated with a single endosome (Figure 6C), suggesting that endosomes may be loaded with multiple mRNAs. However, it does not answer the question whether these originate from the same RBP or from different mRNA attachment systems. The presence of multiple different physical contacts between endosomes and mRNA is consistent with the notion that transcripts can interact with EEs in a translation-dependent or -independent fashion, pointing toward different, yet unknown, regulatory mechanisms.[23] New experimental approaches will have to determine whether the mRNA recruited by the FERRY complex onto EEs is translated.

The role of nuclear-encoded transcripts for mitochondrial proteins

The recruitment of nuclear-encoded mRNAs for mitochondrial proteins to EEs appears redundant for, if not in conflict with, transport of these proteins on LEs.[18] This raises the question about the purpose of different mRNA localization systems for a group of transcripts or a single mRNA and the role of endocytic organelles. Nuclear-encoded transcripts for mitochondrial proteins form a large group of mRNAs that are highly abundant, essential for cell survival, and required in distal sub-compartments of neurons far away from the nucleus. This opens up a variety of possible explanations, ranging from simple redundancy to a division of labor or differential regulation through different transport routes. Organelles of the endolysosomal system exhibit different motility behavior. For example, EEs undergo bidirectional motility along microtubules in both in dendrites and axons.[20] LEs/multi-vesicular bodies move primarily in a retrograde fashion but can also undergo antegrade motility in axons.[21,22,49,50] It seems natural to exploit the different motility behavior not just of LEs and lysosomes but also of EEs to precisely and robustly deliver mRNAs to their respective target location in neuronal processes. Given the duration of endosome movement over long distances in the neuronal processes, it is advantageous that mRNA bound to EEs may be protected from degradation. This hypothesis is supported by transcriptomics analysis showing that the levels of mRNAs encoding mitochondrial proteins are reduced upon KO of FERRY subunits (Figure 5D). Furthermore, it is plausible that the mRNA loaded on EEs may not be translated until its arrival at its destination, e.g., to mitochondria. In view of the complex morphology of neurons and their energy requirement in various sub-compartments, an intricate system to maintain mitochondrial integrity and secure energy supplies is not surprising, and uncovering this system is an interesting future prospect.

Connection between mRNA localization and neurodegeneration

The loss of the ability to regulate mRNA transport and produce proteins locally is detrimental for neuronal survival and brain function. This is also reflected in the large variety of neuronal damage that is caused by genetic disruption of genes connected to mRNA transport such as *fy-1-3*.[34–44] While the causes and consequences of different mutations can be manifold, our data provide a molecular explanation for the deleterious effects in human patients, causing symptoms such as intellectual disability and brain abnormalities.[40] For example, an 84-amino-acid deletion at the C terminus of Fy-2 is sufficient to prevent the interactions between Fy-2 and Fy-1/Fy-3 as well as those of FERRY with Rab5, thus disrupting the structural integrity of the complex and impairing its proper subcellular localization.[33] Clinically relevant truncations of Fy-1 often affect the TBC domain, which is a Rab GTPase-activating protein (GAP) domain that might severely impact endosomal trafficking. Our findings confirm that even small defects in FERRY can affect its capacity in mRNA transport on a large variety of transcripts. Further studies are needed to disentangle the mechanisms by which mRNA mis-localization leads to systemic brain damage.

Limitations of the study

The weak FERRY-mRNA interaction and lack of *in vitro* binding constants seems to be conflicting with the extent of the interface. While we have already discussed possible explanations for the weak interaction, we highlight here the technical limitations for determining reliable *in vitro* binding constants. The structural heterogeneity of the FERRY complex and of the mRNA combined results in conformations that reduce the interactions and impair a proper quantification of active concentrations.

The consequences of the loss of FERRY components on the transcriptome in HeLa cells are difficult to interpret, as they can be caused by different mechanisms, including impaired mRNA localization, but also FERRY-dependent changes in regulation and compensatory effects of the KO. Furthermore, in HeLa cells, mRNA mis-localization can be compensated by diffusion. Performing an in-depth analysis of FERRY-dependent mRNA localization and the effect on local translation in neurons are necessary to step forward. These also require developments in

technology, as our attempts to use published protocols did not succeed.

Overall, this study provides a novel molecular player that, due to its evolutionary conservation and requirement for organism physiology, plays an important role in the intracellular localization and translational control of mRNAs exploiting EEs as a transport system. The identification of the FEERY complex raises a number of questions that need to be addressed in ad hoc structure and function studies. Cells where spatial localization of mRNAs is rate limiting, such as neurons or fungi, are systems of choice to address such questions and test predictions of FERRY complex function.

STAR★METHODS

Detailed methods are provided in the online version of this paper and include the following:

- KEY RESOURCES TABLE
- RESOURCE AVAILABILITY
  - Lead contact
  - Materials availability
  - Data and code availability
- EXPERIMENTAL MODEL AND STUDY PARTICIPANT DETAILS
  - HeLa cell culture
  - HEK 293 cell culture
  - Animals
- METHOD DETAILS
  - Molecular cloning
  - Virus production and insect cell expression
  - Protein purification
  - GST pull-down assay
  - Identifying orthologous sequences
  - Phylogenetic tree estimation
  - FERRY evolution and ancestral state reconstruction
  - Antibody production
  - Antibody validation
  - Antibodies
  - HEK 293 lysate preparation
  - GST-FERRY interactor screens
  - Mass spectrometry
  - Mass photometry
  - Sucrose density gradient centrifugation to analyze ribosome association
  - Library preparation and sequencing
  - Rab5 affinity chromatography
  - *In vitro* translation binding assay
  - mRNA production and electrophoretic motility shift assays
  - RNA immunoprecipitation after UV crosslinking
  - Generation of HeLa KO cell lines
  - RNA extraction from HeLa cells
  - Single molecule fluorescence *in situ* hybridization and immunostaining
  - Preparation of hippocampal cultures
  - Immunostaining of neurons
  - High sensitivity FISH and immunostaining in neurons
  - Microscopy
  - Western blotting
- QUANTIFICATION AND STATISTICAL ANALYSIS
  - Analysis of the mass spectrometry data
  - Analysis of the RNA sequencing data
  - HeLa cell images
  - Neuron images
  - Multiple source localization microscopy

SUPPLEMENTAL INFORMATION

Supplemental information can be found online at https://doi.org/10.1016/j.molcel.2023.05.012.

ACKNOWLEDGMENTS

Firstly, we thank I. Bartnik for excellent technical support and P. Hackert for support with the RNA-IP after crosslinking. We also acknowledge S. Raunser and D. Quentin for valuable feedback regarding the manuscript and the members of the cluster of excellence "Physics of Life" (Deutsche Forschungsgemeinschaft under Germany's Excellence Strategy—EXC-2068–390729961—Cluster of Excellence Physics of Life of Technische Universität Dresden) for discussion. We especially thank the following services and facilities of the MPI-CBG for their support: the antibody facility, the light microscopy facility, the mass spectrometry facility, the genome engineering facility, protein expression and purification facility, and the scientific computing facility. We acknowledge André Gohr for the analysis of RNA-seq data. We also thank the DRESDEN-concept Genome Center (DcGC at CMBC at the TU Dresden) supported by DFG (INST 269/768-1) for technical support. Furthermore, we thank Refeyn, Ltd (Oxford, UK) for the use of their mass photometer. We also thank the Center for Information Services and High Performance Computing (ZIH) of the TU Dresden for the generous provision of computing power. This research was financially supported by the Deutsche Forschungsgemeinschaft (DFG, German Research Foundation)—Project Number 112927078–TRR 83 to M.Z.; Project Number 264061860 - SFB1190 P04 to K.E.B.; and SFB1190, P08/14 to M.T.B.; as well as the Max Planck Society. Open access funding was by the Max Planck Society. J.S.S. was funded by the Deutsche Forschungsgemeinschaft (DFG, German Research Foundation)—Project Number 112927078–TRR 83.

AUTHOR CONTRIBUTIONS

Conceptualization, J.S.S. and M.Z.; Formal analysis, J.S.S., C.L., L.H., Y.K., A.T.-P., and M.Z.; Investigation, J.S.S., S.t.D., S.C., C.L., J.D.G., S.S., R.S., A.G., A.T.-P., K.E.B., M.T.B., and M.Z.; Data curation, J.S.S., L.H., and M.Z.; Writing – original draft, J.S.S. and M.Z.; Writing – review & editing, all authors.; Visualization, J.S.S., C.L., and L.H.; Supervision, J.S.S. and M.Z.; Project administration, J.S.S. and M.Z.; Funding acquisition, K.E.B., M.T.B., E.M.S., and M.Z.

DECLARATION OF INTERESTS

The authors declare no competing interests.

INCLUSION AND DIVERSITY

We support inclusive, diverse, and equitable conduct of research.

Received: July 22, 2022
Revised: December 6, 2022
Accepted: May 8, 2023
Published: June 1, 2023

REFERENCES

1. Cioni, J.M., Koppers, M., and Holt, C.E. (2018). Molecular control of local translation in axon development and maintenance. Curr. Opin. Neurobiol. *51*, 86–94. https://doi.org/10.1016/j.conb.2018.02.025.
2. Glock, C., Heumüller, M., and Schuman, E.M. (2017). mRNA transport & local translation in neurons. Curr. Opin. Neurobiol. *45*, 169–177. https://doi.org/10.1016/j.conb.2017.05.005.
3. Turner-Bridger, B., Caterino, C., and Cioni, J.M. (2020). Molecular mechanisms behind mRNA localization in axons. Open Biol. *10*, 200177. https://doi.org/10.1098/rsob.200177.
4. Martin, K.C., and Ephrussi, A. (2009). mRNA localization: gene expression in the spatial dimension. Cell *136*, 719–730. https://doi.org/10.1016/j.cell.2009.01.044.
5. Das, S., Vera, M., Gandin, V., Singer, R.H., and Tutucci, E. (2021). Intracellular mRNA transport and localized translation. Nat. Rev. Mol. Cell Biol. *22*, 483–504. https://doi.org/10.1038/s41580-021-00356-8.
6. Riechmann, V., and Ephrussi, A. (2001). Axis formation during Drosophila oogenesis. Curr. Opin. Genet. Dev. *11*, 374–383. https://doi.org/10.1016/s0959-437x(00)00207-0.
7. Becalska, A.N., and Gavis, E.R. (2009). Lighting up mRNA localization in Drosophila oogenesis. Development *136*, 2493–2503. https://doi.org/10.1242/dev.032391.
8. Jung, H., Gkogkas, C.G., Sonenberg, N., and Holt, C.E. (2014). Remote control of gene function by local translation. Cell *157*, 26–40. https://doi.org/10.1016/j.cell.2014.03.005.
9. Kim, E., and Jung, H. (2020). Local mRNA translation in long-term maintenance of axon health and function. Curr. Opin. Neurobiol. *63*, 15–22. https://doi.org/10.1016/j.conb.2020.01.006.
10. Briese, M., Saal, L., Appenzeller, S., Moradi, M., Baluapuri, A., and Sendtner, M. (2016). Whole transcriptome profiling reveals the RNA content of motor axons. Nucleic Acids Res. *44*, e33. https://doi.org/10.1093/nar/gkv1027.
11. Andreassi, C., Zimmermann, C., Mitter, R., Fusco, S., De Vita, S., Saiardi, A., and Riccio, A. (2010). An NGF-responsive element targets myo-inositol monophosphatase-1 mRNA to sympathetic neuron axons. Nat. Neurosci. *13*, 291–301. https://doi.org/10.1038/nn.2486.
12. Cajigas, I.J., Tushev, G., Will, T.J., tom Dieck, S., Fuerst, N., and Schuman, E.M. (2012). The local transcriptome in the synaptic neuropil revealed by deep sequencing and high-resolution imaging. Neuron *74*, 453–466. https://doi.org/10.1016/j.neuron.2012.02.036.
13. Baumann, S., Komissarov, A., Gili, M., Ruprecht, V., Wieser, S., and Maurer, S.P. (2020). A reconstituted mammalian APC-kinesin complex selectively transports defined packages of axonal mRNAs. Sci. Adv. *6*, eaaz1588. https://doi.org/10.1126/sciadv.aaz1588.
14. Rodrigues, E.C., Grawenhoff, J., Baumann, S.J., Lorenzon, N., and Maurer, S.P. (2021). Mammalian Neuronal mRNA Transport Complexes: The Few Knowns and the Many Unknowns. Front. Integr. Neurosci. *15*, 692948. https://doi.org/10.3389/fnint.2021.692948.
15. Baumann, S.J., Grawenhoff, J., Rodrigues, E.C., Speroni, S., Gili, M., Komissarov, A., and Maurer, S.P. (2022). APC couples neuronal mRNAs to multiple kinesins, EB1, and shrinking microtubule ends for bidirectional mRNA motility. Proc. Natl. Acad. Sci. USA *119*. e2211536119. https://doi.org/10.1073/pnas.2211536119.
16. Buxbaum, A.R., Haimovich, G., and Singer, R.H. (2015). In the right place at the right time: visualizing and understanding mRNA localization. Nat. Rev. Mol. Cell Biol. *16*, 95–109. https://doi.org/10.1038/nrm3918.
17. Higuchi, Y., Ashwin, P., Roger, Y., and Steinberg, G. (2014). Early endosome motility spatially organizes polysome distribution. J. Cell Biol. *204*, 343–357. https://doi.org/10.1083/jcb.201307164.
18. Cioni, J.M., Lin, J.Q., Holtermann, A.V., Koppers, M., Jakobs, M.A.H., Azizi, A., Turner-Bridger, B., Shigeoka, T., Franze, K., Harris, W.A., and Holt, C.E. (2019). Late Endosomes Act as mRNA Translation Platforms and Sustain Mitochondria in Axons. Cell *176*, 56–72.e15. https://doi.org/10.1016/j.cell.2018.11.030.
19. Liao, Y.C., Fernandopulle, M.S., Wang, G., Choi, H., Hao, L., Drerup, C.M., Patel, R., Qamar, S., Nixon-Abell, J., Shen, Y., et al. (2019). RNA Granules Hitchhike on Lysosomes for Long-Distance Transport, Using Annexin A11 as a Molecular Tether. Cell *179*, 147–164.e20. https://doi.org/10.1016/j.cell.2019.08.050.
20. Goto-Silva, L., McShane, M.P., Salinas, S., Kalaidzidis, Y., Schiavo, G., and Zerial, M. (2019). Retrograde transport of Akt by a neuronal Rab5-APPL1 endosome. Sci. Rep. *9*, 2433. https://doi.org/10.1038/s41598-019-38637-0.
21. Parton, R.G., Simons, K., and Dotti, C.G. (1992). Axonal and dendritic endocytic pathways in cultured neurons. J. Cell Biol. *119*, 123–137. https://doi.org/10.1083/jcb.119.1.123.
22. Cason, S.E., and Holzbaur, E.L.F. (2022). Selective motor activation in organelle transport along axons. Nat. Rev. Mol. Cell Biol. *23*, 699–714. https://doi.org/10.1038/s41580-022-00491-w.
23. Popovic, D., Nijenhuis, W., Kapitein, L.C., and Pelkmans, L. (2020). Co-translational targeting of transcripts to endosomes. Preprint at bioRxiv. https://doi.org/10.1101/2020.07.17.208652.
24. Pfeffer, S.R. (2013). Rab GTPase regulation of membrane identity. Curr. Opin. Cell Biol. *25*, 414–419. https://doi.org/10.1016/j.ceb.2013.04.002.
25. Wandinger-Ness, A., and Zerial, M. (2014). Rab proteins and the compartmentalization of the endosomal system. Cold Spring Harb. Perspect. Biol. *6*, a022616. https://doi.org/10.1101/cshperspect.a022616.
26. Christoforidis, S., McBride, H.M., Burgoyne, R.D., and Zerial, M. (1999). The Rab5 effector EEA1 is a core component of endosome docking. Nature *397*, 621–625. https://doi.org/10.1038/17618.
27. Schnatwinkel, C., Christoforidis, S., Lindsay, M.R., Uttenweiler-Joseph, S., Wilm, M., Parton, R.G., and Zerial, M. (2004). The Rab5 effector Rabankyrin-5 regulates and coordinates different endocytic mechanisms. PLoS Biol. *2*, E261. https://doi.org/10.1371/journal.pbio.0020261.
28. Murray, D.H., Jahnel, M., Lauer, J., Avellaneda, M.J., Brouilly, N., Cezanne, A., Morales-Navarrete, H., Perini, E.D., Ferguson, C., Lupas, A.N., et al. (2016). An endosomal tether undergoes an entropic collapse to bring vesicles together. Nature *537*, 107–111. https://doi.org/10.1038/nature19326.
29. Cezanne, A., Lauer, J., Solomatina, A., Sbalzarini, I.F., and Zerial, M. (2020). A non-linear system patterns Rab5 GTPase on the membrane. Elife *9*, e54434. https://doi.org/10.7554/eLife.54434.
30. Franke, C., Repnik, U., Segeletz, S., Brouilly, N., Kalaidzidis, Y., Verbavatz, J.M., and Zerial, M. (2019). Correlative single-molecule localization microscopy and electron tomography reveals endosome nanoscale domains. Traffic *20*, 601–617. https://doi.org/10.1111/tra.12671.
31. Lippé, R., Miaczynska, M., Rybin, V., Runge, A., and Zerial, M. (2001). Functional synergy between Rab5 effector Rabaptin-5 and exchange factor Rabex-5 when physically associated in a complex. Mol. Biol. Cell *12*, 2219–2228. https://doi.org/10.1091/mbc.12.7.2219.
32. Lauer, J., Segeletz, S., Cezanne, A., Guaitoli, G., Raimondi, F., Gentzel, M., Alva, V., Habeck, M., Kalaidzidis, Y., Ueffing, M., et al. (2019). Auto-regulation of Rab5 GEF activity in Rabex5 by allosteric structural changes, catalytic core dynamics and ubiquitin binding. Elife *8*, e46302. https://doi.org/10.7554/eLife.46302.
33. Quentin, D., Schuhmacher, J., Klink, B.U., Lauer, J., Shaikh, T., Huis in 't Veld, P.J., Welp, L.M., Urlaub, H., Zerial, M., and Raunser, S. (2023). Structural basis of mRNA binding by the human FERRY Rab5 effector complex. Mol. Cell *83*. https://doi.org/10.1016/j.molcel.2023.05.009.
34. Bhoj, E.J., Li, D., Harr, M., Edvardson, S., Elpeleg, O., Chisholm, E., Juusola, J., Douglas, G., Guillen Sacoto, M.J., Siquier-Pernet, K., et al. (2016). Mutations in TBCK, Encoding TBC1-Domain-Containing Kinase, Lead to a Recognizable Syndrome of Intellectual Disability and Hypotonia. Am. J. Hum. Genet. *98*, 782–788. https://doi.org/10.1016/j.ajhg.2016.03.016.

35. Guerreiro, R.J., Brown, R., Dian, D., de Goede, C., Bras, J., and Mole, S.E. (2016). Mutation of TBCK causes a rare recessive developmental disorder. Neurol. Genet. *2*, e76. https://doi.org/10.1212/NXG.0000000000000076.

36. Ortiz-González, X.R., Tintos-Hernández, J.A., Keller, K., Li, X., Foley, A.R., Bharucha-Goebel, D.X., Kessler, S.K., Yum, S.W., Crino, P.B., He, M., et al. (2018). Homozygous boricua TBCK mutation causes neurodegeneration and aberrant autophagy. Ann. Neurol. *83*, 153–165. https://doi.org/10.1002/ana.25130.

37. Chong, J.X., Caputo, V., Phelps, I.G., Stella, L., Worgan, L., Dempsey, J.C., Nguyen, A., Leuzzi, V., Webster, R., Pizzuti, A., et al. (2016). Recessive Inactivating Mutations in TBCK, Encoding a Rab GTPase-Activating Protein, Cause Severe Infantile Syndromic Encephalopathy. Am. J. Hum. Genet. *98*, 772–781. https://doi.org/10.1016/j.ajhg.2016.01.016.

38. Zapata-Aldana, E., Kim, D.D., Remtulla, S., Prasad, C., Nguyen, C.T., and Campbell, C. (2019). Further delineation of TBCK - Infantile hypotonia with psychomotor retardation and characteristic facies type 3. Eur. J. Med. Genet. *62*, 273–277. https://doi.org/10.1016/j.ejmg.2018.08.004.

39. Loddo, S., Alesi, V., Radio, F.C., Genovese, S., Di Tommaso, S., Calvieri, G., Orlando, V., Bertini, E., Dentici, M.L., Novelli, A., and Dallapiccola, B. (2020). PPP1R21-related syndromic intellectual disability: Report of an adult patient and review. Am. J. Med. Genet. *182*, 3014–3022. https://doi.org/10.1002/ajmg.a.61889.

40. Suleiman, J., Al Hashem, A.M., Tabarki, B., Al-Thihli, K., Bi, W., and El-Hattab, A.W. (2018). PPP1R21 homozygous null variants associated with developmental delay, muscle weakness, distinctive facial features, and brain abnormalities. Clin. Genet. *94*, 351–355. https://doi.org/10.1111/cge.13387.

41. Philips, A.K., Pinelli, M., de Bie, C.I., Mustonen, A., Määttä, T., Arts, H.H., Wu, K., Roepman, R., Moilanen, J.S., Raza, S., et al. (2017). Identification of C12orf4 as a gene for autosomal recessive intellectual disability. Clin. Genet. *91*, 100–105. https://doi.org/10.1111/cge.12821.

42. Hancarova, M., Babikyan, D., Bendova, S., Midyan, S., Prchalova, D., Shahsuvaryan, G., Stranecky, V., Sarkisian, T., and Sedlacek, Z. (2019). A novel variant of C12orf4 in a consanguineous Armenian family confirms the etiology of autosomal recessive intellectual disability type 66 with delineation of the phenotype. Mol. Genet. Genomic Med. *7*, e865. https://doi.org/10.1002/mgg3.865.

43. Beck-Wödl, S., Harzer, K., Sturm, M., Buchert, R., Rieß, O., Mennel, H.D., Latta, E., Pagenstecher, A., and Keber, U. (2018). Homozygous TBC1 domain-containing kinase (TBCK) mutation causes a novel lysosomal storage disease - a new type of neuronal ceroid lipofuscinosis (CLN15)? Acta Neuropathol. Commun. *6*, 145. https://doi.org/10.1186/s40478-018-0646-6.

44. Rehman, A.U., Najafi, M., Kambouris, M., Al-Gazali, L., Makrythanasis, P., Rad, A., Maroofian, R., Rajab, A., Stark, Z., Hunter, J.V., et al. (2019). Biallelic loss of function variants in PPP1R21 cause a neurodevelopmental syndrome with impaired endocytic function. Hum. Mutat. *40*, 267–280. https://doi.org/10.1002/humu.23694.

45. Haag, S., Warda, A.S., Kretschmer, J., Günnigmann, M.A., Höbartner, C., and Bohnsack, M.T. (2015). NSUN6 is a human RNA methyltransferase that catalyzes formation of m5C72 in specific tRNAs. RNA *21*, 1532–1543. https://doi.org/10.1261/rna.051524.115.

46. Schieweck, R., Ninkovic, J., and Kiebler, M.A. (2021). RNA-binding proteins balance brain function in health and disease. Physiol. Rev. *101*, 1309–1370.

47. Wilson, J.M., de Hoop, M., Zorzi, N., Toh, B.H., Dotti, C.G., and Parton, R.G. (2000). EEA1, a tethering protein of the early sorting endosome, shows a polarized distribution in hippocampal neurons, epithelial cells, and fibroblasts. Mol. Biol. Cell *11*, 2657–2671. https://doi.org/10.1091/mbc.11.8.2657.

48. Kalaidzidis, Y., Kalaidzidis, I., and Zerial, M. (2015). A Probabilistic Method to Quantify the Colocalization of Markers on Intracellular Vesicular Structures Visualized by Light Microscopy.

49. De Pace, R., Britt, D.J., Mercurio, J., Foster, A.M., Djavaherian, L., Hoffmann, V., Abebe, D., and Bonifacino, J.S. (2020). Synaptic Vesicle Precursors and Lysosomes Are Transported by Different Mechanisms in the Axon of Mammalian Neurons. Cell Rep. *31*, 107775. https://doi.org/10.1016/j.celrep.2020.107775.

50. Farías, G.G., Guardia, C.M., De Pace, R., Britt, D.J., and Bonifacino, J.S. (2017). BORC/kinesin-1 ensemble drives polarized transport of lysosomes into the axon. Proc. Natl. Acad. Sci. USA *114*, E2955–E2964. https://doi.org/10.1073/pnas.1616363114.

51. Schindelin, J., Arganda-Carreras, I., Frise, E., Kaynig, V., Longair, M., Pietzsch, T., Preibisch, S., Rueden, C., Saalfeld, S., Schmid, B., et al. (2012). Fiji: an open-source platform for biological-image analysis. Nat. Methods *9*, 676–682. https://doi.org/10.1038/nmeth.2019.

52. Team, R. (2019). RStudio: Integrated Development for R. (RStudio, Inc.).

53. UniProt Consortium (2019). UniProt: a worldwide hub of protein knowledge. Nucleic Acids Res. *47*, D506–D515. https://doi.org/10.1093/nar/gky1049.

54. Tabari, E., and Su, Z. (2017). PorthoMCL: Parallel orthology prediction using MCL for the realm of massive genome availability. Big Data Anal. *2*, 4. https://doi.org/10.1186/s41044-016-0019-8.

55. Team, R.C. (2019). R: A Language and Environment for Statistical Computing (R Foundation for Statistical Computing).

56. Rozewicki, J., Li, S., Amada, K.M., Standley, D.M., and Katoh, K. (2019). MAFFT-DASH: integrated protein sequence and structural alignment. Nucleic Acids Res. *47*, W5–W10. https://doi.org/10.1093/nar/gkz342.

57. Capella-Gutiérrez, S., Silla-Martínez, J.M., and Gabaldón, T. (2009). trimAl: a tool for automated alignment trimming in large-scale phylogenetic analyses. Bioinformatics *25*, 1972–1973. https://doi.org/10.1093/bioinformatics/btp348.

58. Nguyen, L.T., Schmidt, H.A., von Haeseler, A., and Minh, B.Q. (2015). IQ-TREE: a fast and effective stochastic algorithm for estimating maximum-likelihood phylogenies. Mol. Biol. Evol. *32*, 268–274. https://doi.org/10.1093/molbev/msu300.

59. Chernomor, O., von Haeseler, A., and Minh, B.Q. (2016). Terrace Aware Data Structure for Phylogenomic Inference from Supermatrices. Syst. Biol. *65*, 997–1008. https://doi.org/10.1093/sysbio/syw037.

60. Whelan, S., and Goldman, N. (2001). A general empirical model of protein evolution derived from multiple protein families using a maximum-likelihood approach. Mol. Biol. Evol. *18*, 691–699. https://doi.org/10.1093/oxfordjournals.molbev.a003851.

61. Hoang, D.T., Chernomor, O., von Haeseler, A., Minh, B.Q., and Vinh, L.S. (2018). UFBoot2: Improving the Ultrafast Bootstrap Approximation. Mol. Biol. Evol. *35*, 518–522. https://doi.org/10.1093/molbev/msx281.

62. Yu, G., Smith, D.K., Zhu, H., Guan, Y., and Lam, T.T.-Y. (2017). ggtree: an r package for visualization and annotation of phylogenetic trees with their covariates and other associated data. Methods Ecol. Evol. *8*, 28–36. https://doi.org/10.1111/2041-210X.12628.

63. Yu, G., Lam, T.T.Y., Zhu, H., and Guan, Y. (2018). Two Methods for Mapping and Visualizing Associated Data on Phylogeny Using Ggtree. Mol. Biol. Evol. *35*, 3041–3043. https://doi.org/10.1093/molbev/msy194.

64. Pagel, M. (1994). Detecting Correlated Evolution on Phylogenies: A General Method for the Comparative Analysis of Discrete Characters. Proceedings of the Royal Society of London Series B *255*, 37.

65. Paradis, E., and Schliep, K. (2019). ape 5.0: an environment for modern phylogenetics and evolutionary analyses in R. Bioinformatics *35*, 526–528. https://doi.org/10.1093/bioinformatics/bty633.

66. Sleister, H.M., and Rao, A.G. (2001). Strategies to generate antibodies capable of distinguishing between proteins with >90% amino acid identity. J. Immunol. Methods *252*, 121–129. https://doi.org/10.1016/s0022-1759(01)00346-5.

67. Chiva, C., Olivella, R., Borràs, E., Espadas, G., Pastor, O., Solé, A., and Sabidó, E. (2018). QCloud: A cloud-based quality control system for

mass spectrometry-based proteomics laboratories. PLoS One *13*, e0189209. https://doi.org/10.1371/journal.pone.0189209.

68. Cox, J., and Mann, M. (2008). MaxQuant enables high peptide identification rates, individualized p.p.b.-range mass accuracies and proteome-wide protein quantification. Nat. Biotechnol. *26*, 1367–1372. https://doi.org/10.1038/nbt.1511.
69. Young, G., Hundt, N., Cole, D., Fineberg, A., Andrecka, J., Tyler, A., Olerinyova, A., Ansari, A., Marklund, E.G., Collier, M.P., et al. (2018). Quantitative mass imaging of single biological macromolecules. Science *360*, 423–427. https://doi.org/10.1126/science.aar5839.
70. Jaafar, M., Contreras, J., Dominique, C., Martín-Villanueva, S., Capeyrou, R., Vitali, P., Rodríguez-Galán, O., Velasco, C., Humbert, O., Watkins, N.J., et al. (2021). Association of snR190 snoRNA chaperone with early pre-60S particles is regulated by the RNA helicase Dbp7 in yeast. Nat. Commun. *12*, 6153. https://doi.org/10.1038/s41467-021-26207-w.
71. Aquino, G.R.R., Hackert, P., Krogh, N., Pan, K.T., Jaafar, M., Henras, A.K., Nielsen, H., Urlaub, H., Bohnsack, K.E., and Bohnsack, M.T. (2021). The RNA helicase Dbp7 promotes domain V/VI compaction and stabilization of inter-domain interactions during early 60S assembly. Nat. Commun. *12*, 6152. https://doi.org/10.1038/s41467-021-26208-9.
72. Nielsen, E., Christoforidis, S., Uttenweiler-Joseph, S., Miaczynska, M., Dewitte, F., Wilm, M., Hoflack, B., and Zerial, M. (2000). Rabenosyn-5, a novel Rab5 effector, is complexed with hVPS45 and recruited to endosomes through a FYVE finger domain. J. Cell Biol. *151*, 601–612. https://doi.org/10.1083/jcb.151.3.601.
73. Choudhury, P., Hackert, P., Memet, I., Sloan, K.E., and Bohnsack, M.T. (2019). The human RNA helicase DHX37 is required for release of the U3 snoRNP from pre-ribosomal particles. RNA Biol. *16*, 54–68. https://doi.org/10.1080/15476286.2018.1556149.
74. Memet, I., Doebele, C., Sloan, K.E., and Bohnsack, M.T. (2017). The G-patch protein NF-kappaB-repressing factor mediates the recruitment of the exonuclease XRN2 and activation of the RNA helicase DHX15 in human ribosome biogenesis. Nucleic Acids Res. *45*, 5359–5374. https://doi.org/10.1093/nar/gkx013.
75. Sloan, K.E., Leisegang, M.S., Doebele, C., Ramírez, A.S., Simm, S., Safferthal, C., Kretschmer, J., Schorge, T., Markoutsa, S., Haag, S., et al. (2015). The association of late-acting snoRNPs with human pre-ribosomal complexes requires the RNA helicase DDX21. Nucleic Acids Res. *43*, 553–564. https://doi.org/10.1093/nar/gku1291.
76. Spiegel, A., Bachmann, M., Jurado Jiménez, G., and Sarov, M. (2019). CRISPR/Cas9-based knockout pipeline for reverse genetics in mammalian cell culture. Methods *164–165*, 49–58. https://doi.org/10.1016/j.ymeth.2019.04.016.
77. Kaech, S., and Banker, G. (2006). Culturing hippocampal neurons. Nat. Protoc. *1*, 2406–2415. https://doi.org/10.1038/nprot.2006.356.
78. Preibisch, S., Saalfeld, S., and Tomancak, P. (2009). Globally optimal stitching of tiled 3D microscopic image acquisitions. Bioinformatics *25*, 1463–1465. https://doi.org/10.1093/bioinformatics/btp184.
79. Zhang, X., Smits, A.H., van Tilburg, G.B., Ovaa, H., Huber, W., and Vermeulen, M. (2018). Proteome-wide identification of ubiquitin interactions using UbIA-MS. Nat. Protoc. *13*, 530–550. https://doi.org/10.1038/nprot.2017.147.
80. Huber, W., von Heydebreck, A., Sültmann, H., Poustka, A., and Vingron, M. (2002). Variance stabilization applied to microarray data calibration and to the quantification of differential expression. Bioinformatics *18* (*Suppl 1*), S96–S104. https://doi.org/10.1093/bioinformatics/18.suppl_1.s96.
81. Gatto, L., Gibb, S., and Rainer, J. (2021). MSnbase, Efficient and Elegant R-Based Processing and Visualization of Raw Mass Spectrometry Data. J. Proteome Res. *20*, 1063–1069. https://doi.org/10.1021/acs.jproteome.0c00313.
82. Ritchie, M.E., Phipson, B., Wu, D., Hu, Y., Law, C.W., Shi, W., and Smyth, G.K. (2015). limma powers differential expression analyses for RNA-sequencing and microarray studies. Nucleic Acids Res. *43*, e47. https://doi.org/10.1093/nar/gkv007.
83. Andrews, S. (2010). FastQC: A Quality Control Tool for High Throughput Sequence Data.
84. Yates, A.D., Achuthan, P., Akanni, W., Allen, J., Allen, J., Alvarez-Jarreta, J., Amode, M.R., Armean, I.M., Azov, A.G., Bennett, R., et al. (2020). Ensembl 2020. Nucleic Acids Res. *48*, D682–D688. https://doi.org/10.1093/nar/gkz966.
85. Dobin, A., Davis, C.A., Schlesinger, F., Drenkow, J., Zaleski, C., Jha, S., Batut, P., Chaisson, M., and Gingeras, T.R. (2013). STAR: ultrafast universal RNA-seq aligner. Bioinformatics *29*, 15–21. https://doi.org/10.1093/bioinformatics/bts635.
86. Love, M.I., Huber, W., and Anders, S. (2014). Moderated estimation of fold change and dispersion for RNA-seq data with DESeq2. Genome Biol. *15*, 550. https://doi.org/10.1186/s13059-014-0550-8.
87. Ignatiadis, N., Klaus, B., Zaugg, J.B., and Huber, W. (2016). Data-driven hypothesis weighting increases detection power in genome-scale multiple testing. Nat. Methods *13*, 577–580. https://doi.org/10.1038/nmeth.3885.
88. Wickham, H. (2016). ggplot2: Elegant Graphics for Data Analysis.
89. Kassambara, A. (2020). ggpubr: 'ggplot2 (Based Publication Ready Plots).
90. Dolgalev, I. (2020). msigdbr: MSigDB Gene Sets for Multiple Organisms in a Tidy Data Format. R package version 7.2.1. https://CRAN.R-project.org/package=msigdbr.
91. Korotkevich, G., Sukhov, V., Budin, N., Shpak, B., Artyomov, M.N., and Sergushichev, A. (2021). Fast gene set enrichment analysis. Preprint at bioRxiv. https://doi.org/10.1101/060012.
92. Subramanian, A., Tamayo, P., Mootha, V.K., Mukherjee, S., Ebert, B.L., Gillette, M.A., Paulovich, A., Pomeroy, S.L., Golub, T.R., Lander, E.S., and Mesirov, J.P. (2005). Gene set enrichment analysis: a knowledge-based approach for interpreting genome-wide expression profiles. Proc. Natl. Acad. Sci. USA *102*, 15545–15550. https://doi.org/10.1073/pnas.0506580102.
93. Yu, G., Wang, L.G., Han, Y., and He, Q.Y. (2012). clusterProfiler: an R package for comparing biological themes among gene clusters. OMICS *16*, 284–287. https://doi.org/10.1089/omi.2011.0118.
94. Yu, G., and He, Q.Y. (2016). ReactomePA: an R/Bioconductor package for reactome pathway analysis and visualization. Mol. Biosyst. *12*, 477–479. https://doi.org/10.1039/c5mb00663e.
95. Durinck, S., Spellman, P.T., Birney, E., and Huber, W. (2009). Mapping identifiers for the integration of genomic datasets with the R/Bioconductor package biomaRt. Nat. Protoc. *4*, 1184–1191. https://doi.org/10.1038/nprot.2009.97.
96. Collinet, C., Stöter, M., Bradshaw, C.R., Samusik, N., Rink, J.C., Kenski, D., Habermann, B., Buchholz, F., Henschel, R., Mueller, M.S., et al. (2010). Systems survey of endocytosis by multiparametric image analysis. Nature *464*, 243–249. https://doi.org/10.1038/nature08779.
97. Agarwal, K., and Macháň, R. (2016). Multiple signal classification algorithm for super-resolution fluorescence microscopy. Nat. Commun. *7*, 13752. https://doi.org/10.1038/ncomms13752.

STAR★METHODS

KEY RESOURCES TABLE

REAGENT or RESOURCE	SOURCE	IDENTIFIER
Antibodies		
Rab5 monoclonal antibody	BD Bioscience	Cat# 610725; RRID:AB_398048
Map2 polyclonal antibody	Merck/Chemicon	Cat# AB5622; RRID: AB_91939
Map2 polyclonlal antiserum	Synaptic systems	Cat# 188004; RRID:AB_2138181
Phospho-NF-H monoclonal antibody	Biolegend	Cat# 801602; RRID:AB_2715851
TOMM70A polyclonal antibody	Proteintech	14528-1-AP; RRID:AB_2303727
Fy-1 polyclonal antibody	Sigma Aldrich	Cat# HPA039951; RRID:AB_10795300
Fy-3 polyclonal antibody	Sigma Aldrich	Cat# HPA037871; RRID:AB_10670531
GAPDH monoclonal antibody	Sigma Aldrich	Cat# G8795; RRID:AB_1078991
EEA1 polyclonal antibody	this study	N/A
Rabankyrin-5 monoclonal antibody	this study	N/A
Fy-2 monoclonal antibody	this study	N/A
Fy-4 polyclonal antibody	this study	N/A
Fy-5 monoclonal antibody	this study	N/A
Mdh2 polyclonal antibody	Atlas antibodies	Cat# HPA019714; RRID:AB_1853678
Mrpl41 polyclonal antibody	Atlas antibodies	Cat# HPA024550; RRID:AB_1854112
Flag M2 monoclonal antibody	Sigma Aldrich	Cat# F3165; RRID:AB_259529
RPL3 polyclonal antibody	Proteintech	Cat# 11005-1-AP; RRID:AB_2181760
RPS3A polyclonal antibody	Proteintech	Cat# 14123-1-AP; RRID:AB_2253921
Goat anti-Rat IgG (H + L) Highly Cross-Adsorbed Secondary Antibody, Alexa Fluor 488	Thermo Fisher	Cat# A-11006; RRID:AB_2534074
Goat anti-Mouse IgG (H + L) Highly Cross-Adsorbed Secondary Antibody, Alexa Fluor 568	Thermo Fisher	Cat# A-11031; RRID:AB_144696
Goat anti-Mouse IgG (H + L) Cross-Adsorbed Secondary Antibody, Alexa Fluor 405	Thermo Fisher	Cat# A-31553; RRID:AB_221604
Goat anti-Rabbit IgG (H + L) Cross-Adsorbed Secondary Antibody, Alexa Fluor 647	Thermo Fisher	Cat# A-21244; RRID:AB_2535812
F(ab')2-Goat anti-Rabbit IgG (H + L) Cross-Adsorbed Secondary Antibody, Alexa Fluor 647	Thermo Fisher	Cat# A-21246; RRID:AB_2535814
Goat anti-Mouse IgG (H + L) Cross-Adsorbed Secondary Antibody, Alexa Fluor 488	Thermo Fisher	Cat# A-11001; RRID:AB_2534069
Bacterial and virus strains		
E. coli DH5a	In-house made	N/A
E. coli BL21 (DE3)	In-house made	N/A
Chemicals, peptides, and recombinant proteins		
Iodixanol (OptiPrep Density Gradient Medium)	Merck	Cat# D1556-250mL
D-(+)-Sucrose, pure, pharma grade	Applichem	Cat# A1125.1000
DMEM	Gibco	Cat# 31960-021
fetal bovine serum (FBS)	Gibco	Cat# 10500-064
Penicillin-Streptomycin	Gibco	Cat# 15140-122
FreeStyle™ 293 Expression Medium	Thermo Fisher Scientific	Cat# 12338018
ESF 921 Insect Cell Culture Medium	Expression Systems	Cat# 96-001
Glutathione Sepharose 4B	Cytiva	Cat# 170756

(*Continued on next page*)

Continued

REAGENT or RESOURCE	SOURCE	IDENTIFIER
Guanosine 5′-triphosphate	Merck	Cat# G8877
guanosine 5′-*O*-[gamma-thio]triphosphate	Merck	Cat# G8634
Guanosine 5′-diphosphate	Merck	Cat# G7127
SYBR™ Gold Nucleic Acid Gel Stain	Invotrogen	Cat# S33102
SYPRO Red Protein Gel Stain	Invotrogen	Cat# S6654
RNace-It	Agilent technologies	Cat# 400720
cOmplete-EDTA-free protease inhibitors	Roche	Cat# 4693132001
anti-Flag M2 beads	Sigma Aldrich	Cat# M8823
Ni-NTA agarose beads	Qiagen	Cat# 30210
4-thiouridine	Sigma Aldrich	Cat# T4509
Cas9 protein	IDT	Cat# 1081061
tracrRNA	IDT	Cat# 1072534
Trypsin	Promega	Cat# VA9000
Triton X-100	Serva	Cat# 37340.01
Aqua-Poly/Mount	Polysciences	Cat# 18606
TetraSpeck™ Microspheres	Thermo Fisher	Cat# T7279
ECL™ Western Blotting Reagents	Cytiva	Cat# RPN2106
Neurobasal A medium	Thermo Fisher Scientific (Gibco)	Cat# 10888-022
B27 medium	Thermo Fisher Scientific (Gibco)	Cat# 17504044
Glutamax	Thermo Fisher Scientific	Cat# 350-50038
Dithiotritol (DTT)	Merck	Cat# D5545
Critical commercial assays		
bicinchoninic acid assay (BCA)	Pierce BCA Protein Assay Kit (Thermo Scientific)	Cat#23225
T7 RiboMAX™ Express Large Scale RNA Production System	Promega	Cat# P1320
QIAprep Spin Miniprep Kit	Qiagen	Cat# 27106
QIAquick PCR Purification Kit	Qiagen	Cat# 28106
QIAEX II Gel Extraction Kit	Qiagen	Cat# 20021
ViewRNA ISH Cell Assay Kit	Thermo Fisher	Cat# QVC0001
NEBNext rRNA depletion Kit (human, mouse, rat)	New England Biolabs	Cat# E6310
NEBNext Ultra II Directional RNA Library Prep	New England Biolabs	Cat# E7760
TnT™ coupled transcription–translation kit	Promega	Cat# L1170
QuickExtract DNA extraction kit	Epicentre	Cat# QER090150
RNeasy® MinElute® Cleanup Kit	Qiagen	Cat# 74204
Deposited data		
RNASeq: GST-FERRY mRNA pull-down	this study	GEO: GSE173422
RNASeq: Transcriptome of FERRY component KO cell lines	this study	GEO: GSE230114
Analysis pipeline of proteomics and RNASeq data	this study	Github: https://dx.doi.org/21.11101/0000-0007-EEE3-D
Original gels, blots, and microscopy images used in figures	this study	Mendeley data: https://doi.org/10.17632/5dt5pg5jdj.2
Experimental models: Cell lines		
SF9 cells	expression systems	Cat# 94-001F
HeLa Kyoto	This paper	N/A
Primary Rat neurons	Isolated in-house	N/A

(*Continued on next page*)

Continued

REAGENT or RESOURCE	SOURCE	IDENTIFIER
FreeStyle™ 293-F Cells	Sigma Aldrich	Cat# K900010
Stably transfected HEK293 Flp-In T-Rex cell line for expression of 2xFlag-Pre-Scission protease cleavage site-His_6-Fy-2	this study	N/A
Stably transfected HEK293 Flp-In T-Rex cell line for expression of Fy-2-His_6-Pre-Scission protease cleavage site-2xFlag	this study	N/A
Stably transfected HEK293 Flp-In T-Rex cell line for expression of 2xFlag-Pre-Scission protease cleavage site-His_6	this study	N/A
Experimental models: Organisms/strains		
CD® (Sprague Dawley) IGS Rat (Crl:CD(SD))	Charles River	RRID: RGD_734476
RjHan:WI - Wistar rats (Male and female)	Janvier	RRID: RGD_13508588
Oligonucleotides		
See Table S3: Additional resources – Sequence information for oligonucleotides and sequences of *in vitro* transcribed mRNA	this study	N/A
Recombinant DNA		
Fy-5 (N-His, pOCC1)	this study	N/A
Fy-4 (N-His, pOCC5)	this study	N/A
Fy-1 (N-HIs), Fy-2 and Fy-3 (pOEM, multi-gene construct)	this study	N/A
Fy-1, Fy-2 (N-GST) and Fy-3 (pOEM, multi-gene construct)	this study	N/A
Rab5a (N-His, N-GST, pGAT2)	this study	N/A
GST-Rab5a (N-GST, pGEX-6P-3)	this study	N/A
Fy-2 (N-2xFlag-His_6; pcDNA5-derivative)	this study	N/A
Fy-2 (C-His_6-2xFlag; pcDNA5-derivative)	this study	N/A
Flag-His (pcDNA5-derivative)	Markus T. Bohnsack	pMB187
pUC57 syn-*mrpl41*-mRNA	this study	N/A
pUC57 syn-*mdh2*-mRNA	this study	N/A
pUC57 syn-*prdx5*-mRNA	this study	N/A
pUC57 syn-*pigl*-mRNA	this study	N/A
pUC57 syn-gstp1-mRNA	this study	N/A
pUC57 syn-*uchl1*-mRNA	this study	N/A
pUC57 syn-*atp5f1b*-mRNA	this study	N/A
pUC57 syn-*cox6b*-mRNA	this study	N/A
pUC57 syn-*cox8a*-mRNA	this study	N/A
pUC57 syn-*mrpl41*-5′UTR-mRNA	this study	N/A
pUC57 syn-*mrpl41*-orf-mRNA	this study	N/A
pUC57 syn-*mrpl41*-3′UTR-50A-mRNA	this study	N/A
pUC18 syn-*mdh2*-5′UTR-orf-mRNA	this study	N/A
pUC18 syn-*mdh2*-3′UTR-50A-mRNA	this study	N/A
pUC18 syn-*atp5f1b*-5′UTR-orf-mRNA	this study	N/A
pUC18 syn-*atp5f1b*-3′UTR-50A-mRNA	this study	N/A
pUC18 syn-*uchl1*-5′UTR-orf-mRNA	this study	N/A
pUC18 syn-*uchl1*-3′UTR-50A-mRNA	this study	N/A
$tRNA^{Arg(ACG)}$ (pQE80-derivative; pMB920)	Haag et al. 2015[45]	pMB920

(*Continued on next page*)

Continued

REAGENT or RESOURCE	SOURCE	IDENTIFIER
tRNACys$^{(GCA)}$ (pQE80-derivative; pMB921)	Haag et al. 2015[45]	pMB921
tRNA$^{Phe(GAA)}$ (pQE80-derivative; pMB922)	Haag et al. 2015[45]	pMB922
Software and algorithms		
Fiji	Schindelin et al. 2012[51]	https://fiji.sc; RRID:SCR_002285
Motion Tracking	Yannis Kalaidzidis	http://motiontracking.mpi-cbg.de/get/
R version R 3.6.1	R core team	https://www.r-project.org; RRID:SCR_001905
R Studio	RStudio Team	https://www.rstudio.com; RRID:SCR_000432
MaxQuant software package Version 1.6.10.43	available online	https://www.maxquant.org.; RRID:SCR_014485
DiscoverMP software	Refeyn	N/A

RESOURCE AVAILABILITY

Lead contact

Further information and requests for resources and reagents should be directed to and will be fulfilled by the lead contact, Marino Zerial (zerial@mpi-cbg.de).

Materials availability

Material generated in this study is available from the lead contact.

Data and code availability

- RNA-seq data have been deposited to the GEO database and are publicly available as of the date of publication. Accession numbers are listed in the key resources table.
- This paper does not report original code. Custom-built pipelines were used for the analysis of the proteomics and RNASeq data. The respective scripts for the analysis of the RNA-seq and proteomics data are available in a public repository (https://dx.doi.org/21.11101/0000-0007-EEE3-D). All tools used for analysis are referenced in the section 'quantification and statistical analysis'.
- Any additional information required to reanalyze the data reported in this paper is available from the lead contact upon request.

EXPERIMENTAL MODEL AND STUDY PARTICIPANT DETAILS

HeLa cell culture

Hela Kyoto and FERRY subunit knockout cells were cultured in DMEM media supplemented with 10% FBS Superior (Merck) and 50 μg/mL streptomycin (P/S) (Gibco) at 37°C with 5% CO_2. For smFISH studies, cells were seeded into 384 well plates at a density of 3000 cells/well in 50 μL using the drop dispenser (Multidrop, Thermo Fischer Scientific) and cultured for 24h.

HEK 293 cell culture

FreeStyle 293-F Cells (Thermo Fisher Scientific) were grown in suspension culture in FreeStyle 293 Expression Medium (Thermo Fisher Scientific).

Animals

The rat pups were used without gender determination. Timed pregnant rats were purchased from either Janvier labs (RjHan:WI - Wistar rats) or Charles River Laboratories (CD (Sprague Dawley) IGS Rat (Crl:CD(SD))), maintained under food and water *ad libitum* in a 12h–12h light dark cycle. Hippocampal neurons were either isolated from embryos at E17 or P0/P1 SD rats of either sex (see method details). The animals were sacrificed by decapitation with sharp scissors before dissection of the tissue. The procedures involving animal treatment and care were conducted in conformity with the institutional guidelines that are in compliance with the national and international laws and policies (DIRECTIVE2010/63/EU; German animal welfare law, FELASA guidelines) and approved by and reported to the local governmental supervising authorities (Regierungspräsidium Darmstadt and Landesdirektion Sachsen). The animals were euthanized according to annex 2 of §2 Abs. 2 Tierschutz-Versuchstier-Verordnung.

METHOD DETAILS

Molecular cloning

Human *fy-1* (Tbck, ENSG00000145348, Q8TEA7), *fy-2* (Ppp1r21, ENSG00000162869, Q6ZMI0), *fy-3* (C12orf4, ENSG00000047621, Q9NQ89), *fy-4* (Cryzl1, ENSG00000205758, O95825), *fy-5* (Gatd1, ENSG00000177225, Q8NB37) and *rab5a* (ENSG00000144566, P20339), were amplified by polymerase chain reaction (PCR) using Q5 High-Fidelity DNA polymerase (NEB) and digested using NotI, NcoI, AscI, XhoI, PciI (NEB) according to the manufacturer's protocol. *fy-5* was cloned into a pET based bacterial expression vector as an N-terminally hexahistidine (His_6) tagged variant without cleavage site. *fy-4* was cloned into an expression vector for expression in SF9 cells also carrying a non-cleavable N-terminal His_6 tag. *fy-1*, *fy-2* and *fy-3* were cloned into a multi gene construct based on a pBLA vector. For the purification of the FERRY complex *fy-1* carried a cleavable N-terminal His_6 tag, the other 2 genes were untagged. To obtain GST-FERRY, *fy-2* carried a cleavable Glutathione-S-transferase (GST) tag, while *fy-1* and *fy-3* remained untagged. *rab5* was used as GST fusion variant in the bacterial expression vectors pGAT2 for GST pulldown assays and pGEX-6P-3 for electrophoretic mobility shift assays (EMSAs). Plasmids and primers used in this study are listed in the key resources table (Table S3).

Virus production and insect cell expression

SF9 cells growing in ESF921 medium (Expression Systems) were co-transfected with linearized viral genome and the expression plasmid, and selected for high infectivity. P1 and P2 viruses were generated according to the manufacturer's protocol. Best viruses were used to infect SF9 cells at 10^6 cells/ml at 1% v/v and routinely harvested after around 48 h at about $1.5x10^6$ cells/ml. The pellet was suspended in lysis buffer (20 mM HEPES (pH 7.5), 250 mM NaCl, 20 mM KCl, 20 mM $MgCl_2$ and 40 mM imidazole) or SEC buffer (20mM HEPES, pH 7.5, 250mM NaCl, 20mM KCl, 20mM $MgCl_2$) supplemented with a protease inhibitor cocktail, flash frozen in liquid nitrogen and stored at −80°.

Protein purification

Fy-5 and GST-Rab5

For expression of Fy-5 and GST-Rab5, *E. coli* BL21 (DE3) (company) were grown in LB medium under autoinduction conditions using D-(+)-lactose monohydrate at 1.75% (w/v), supplemented with the respective antibiotic (50 μg/mL kanamycin or100 μg/ml ampicillin) at 30°C under constant shaking (165 rpm). Bacteria were harvested by centrifugation (4000 x g, 20 min, 4°C), suspended in lysis buffer and subsequently lysed or stored at −80°C. After sonication the lysate was clarified by centrifugation (22 500 rpm/61 236 x *g*, 20 min, 4°C) and applied to a HisTrap FF column (GE Healthcare) equilibrated with 10 column volumes (CV) of lysis buffer. After extensive washing with lysis buffer, the proteins were eluted in 10–13 mL elution buffer (20 mM HEPES (pH 7.5), 250 mM NaCl, 20 mM KCl, 20 mM $MgCl_2$ and 500 mM imidazole). Elution fractions containing protein were concentrated using Amicon Ultracel-10K/ Ultracel-30K (Millipore) centrifuge filters and subsequently applied to size exclusion chromatography (SEC) using a Superdex 200 column (HiLoad 16/600 Superdex 200 pg, GE Healthcare) equilibrated in SEC buffer. Fractions were analyzed using SDS-PAGE. Protein containing fractions were pooled and concentrated to fit experimental requirements. Protein concentrations were determined by spectrophotometer (NanoDrop Lite, Thermo Scientific).

Fy-4

For expression of Fy-4, insect cell suspensions were lysed using sonication, the lysate subsequently clarified by centrifugation (22 500 rpm/61 236 x *g*, 20 min, 4°C), filtrated using Millex HV membrane filter units with a pore size of 0.45 μm (Merck Millipore) and applied to a HisTrap FF column (GE Healthcare) equilibrated with 10 CV of lysis buffer. After washing with lysis buffer, the protein was eluted in 10–13 mL elution buffer and concentrated with a centrifuge filter (Amicon Ultracel-30K, Millipore). Thereafter, the protein was applied to SEC using a Superdex 200 column (HiLoad 16/600 Superdex 200 pg, GE Healthcare) equilibrated in SEC buffer. The fractions were analyzed by SDS-PAGE. Protein containing fractions were pooled and concentrated according to experimental requirements. The protein concentration was determined by spectrophotometer (NanoDrop Lite, Thermo Scientific).

FERRY complex

SF9 cell pellets prior infected with a virus containing Fy-1, Fy-2 and Fy-3 were melted and immediately supplemented with an excess of purified Fy-4 and Fy-5 before lysis. Subsequently, the cells were lysed using a Microfluidizer (LM20, Microfluidics). The lysate was clarified by centrifugation (22 500 rpm/61 236 x *g*, 20 min, 4°C) and filtrated using membrane filters with a pore size of 0.45 μm (Millex HV membrane filter units, Merck Millipore). The clarified lysate was supplemented with Ni-NTA agarose (1.3 mL resin/1 L insect cell pellet, Qiagen) and incubated for 30 min at 4°C on a rotating wheel. Subsequently, the resin was transferred into gravity flow chromatography columns (Poly-Prep Chromatography Column, Bio-Rad) and washed 3 times with i) 8 CV lysis buffer, ii) 8 CV wash buffer (20 mM HEPES, pH 7.5, 250 mM NaCl, 20 mM KCl, 20 mM $MgCl_2$ and 80 mM imidazole), and iii) 8 CV lysis buffer. The protein was eluted in 1 mL fractions with elution buffer and protein containing fractions were applied to SEC without further concentration, using either a Superdex 200 (HiLoad 16/600 Superdex 200 pg, GE Healthcare) or a Superose 6 increase (Superose 6 Increase 10/300 GL, GE Healthcare) which were equilibrated in SEC buffer. Protein containing fractions were pooled and concentrated according to experimental requirements. Concentration was determined by a spectrophotometer (NanoDrop Lite, Thermo Scientific) and the SEC profile visualized using RStudio.[52]

GST-FERRY complex

SF9 cell pellets prior infected with a virus containing Fy-1, GST-Fy-2 and Fy-3 were melted and immediately supplemented with an excess of purified Fy-4 and Fy-5. The cells were lysed using a Microfluidizer (LM20, Microfluidics), the lysate was clarified by centrifugation (22 500 rpm/61 236 x *g*, 20 min, 4°C) and subsequently filtrated using membrane filters with a pore size of 0.45 μm (Millex HV membrane filter units, Merck Millipore). The clarified lysate was supplemented with Glutathione Sepharose 4B (Cytiva, 2.2 mL resin/1 L insect cell pellet) and incubated for 1.5 h at 4°C on a rotating wheel. The beads were washed once with 10 mL SEC buffer supplemented with purified Fy-4 and 5 and 2 times with 10 mL SEC buffer. To elute the GST-FERRY complex, the beads were incubated with GSH buffer (20 mM HEPES (pH 7.5), 250 mM NaCl, 20 mM KCl, 20 mM $MgCl_2$, 20 mM GSH) for 1.5 h at 4°C on a rotating wheel and the beads were removed using filter columns (MoBiTec). The protein complex was concentrated using centrifuge filters (Amicon Ultracel-30K, Millipore) and subjected to SEC using a Superdex 200 column (HiLoad 16/600 Superdex 200 pg, GE Healthcare) equilibrated in SEC buffer. Protein containing fractions were pooled and concentrated according to experimental requirements. Concentration was determined by a spectrophotometer (NanoDrop Lite, Thermo Scientific)

Rab5:GTPγS

Expression of Rab5a was performed under autoinduction conditions as described before (Fy-5 and GST-Rab5). Harvested bacterial pellets were resuspended in SEC buffer and lysed using sonication. Glutathione Sepharose 4B (Cytiva) was added to the clarified lysate and incubated for 1.5 h at 4°C. The resin was washed 3 times with SEC buffer and the protein cleaved off the resin using HRV 3C protease (produced in house) at 4°C over night on a rotating wheel. Afterward, the protein was concentrated using Amicon Ultracel-30K (Millipore) centrifuge filters and subsequently applied to SEC using a Superdex 200 column (HiLoad 16/600 Superdex 200 pg, GE Healthcare) equilibrated in SEC buffer. Fractions were analyzed using SDS-PAGE. Protein containing fractions were pooled and concentrated according to experimental requirements. The protein concentration was determined by a spectrophotometer (NanoDrop Lite, Thermo Scientific).

For the nucleotide loading, Rab5 was concentrated using an Amicon Ultracel-30K (Millipore) centrifuge filter, subsequently supplemented with 2.5 mM GTPγS and 250 nM of a GST fusion of the Rab5 GEF domain of Rabex5 (GST-Rabex5-Vps9) and incubated for 1 h on ice. To remove the Rab5 GEF domain, Glutathione Sepharose 4B (Cytiva) was added to the mixture and incubated for 1.5 h at 4°C. The resin was pelleted by centrifugation (12 000 rpm/15 300 x g, 10 min, 4°C) and the supernatant containing the GTPγS loaded Rab5 was flash frozen and stored at −80°C. The protein concentration was determined using a BCA assay (Pierce BCA Protein Assay Kit, Thermo Scientific).

GST pull-down assay

5nmol of purified GST-Rab5 was incubated with 12 μL Glutathione Sepharose 4B (Cytiva) in 100 μL SEC buffer in small filter columns (MoBiTec) for 60 min at 4°C moderately shaking (700 rpm) in order to saturate the beads with GST protein. Subsequent centrifugation (2500 rpm/660 x *g*, 1 min, 4°C) removed unbound protein and the resin was washed once with 100 μL SEC buffer. For nucleotide exchange, 1 mM nucleotide (GDP or GTPγS) and 420 nM of GST-Rabex5-Vps9 was added to the columns in 100 μL SEC buffer and incubated for 60 min at 4°C moderately shaking (700 rpm). After centrifugation (2500 rpm/660 x *g*, 1 min, 4°C) and subsequent washing with 100 μL SEC buffer, 0.1 nmol FERRY complex was added to the columns in 100 μL SEC buffer and incubated for 20 min at 4°C on a shaker (700 rpm). Again, unbound protein was removed by centrifugation (2500 rpm/660 x *g*, 1 min, 4°C) and the columns were washed 3 times with 100 μL SEC buffer. Proteins were eluted with 40 μL of GSH buffer (SEC buffer with 20 mM GSH) for 40 min at 4°C on a shaker (700 rpm) and analyzed by SDS-PAGE and Western blotting.

Identifying orthologous sequences

We downloaded all eukaryotic reference proteomes from uniport (last accessed: March 2nd 2020).[53] We used PorthoMCL[54] to identify orthologous clusters containing human FERRY components (GALD1_HUMAN, QORL1_HUMAN, CL004_HUMAN, PPR21_HUMAN, TBCK_HUMAN). Sequences deviating strongly in length from their human homolog were removed (Table S1). We further distinguished PPR21_HUMAN orthologs between sequences which contain a Fy-4 and a Fy-5 binding site and sequences which do not. For the detection of the presence of the Fy-4 and the Fy-5 binding sites, we aligned all identified Fy-2 sequences. We considered the binding sites present if all of the regions aligned to the PPR21_HUMAN binding regions contained less than 20% gaps (ignoring gapped sites in PPR21_HUMAN).

Phylogenetic tree estimation

All orthologous clusters were scanned for species which contain at least 80% of identified species with FERRY proteins (custom R script; R 3.6.1; R Core[55]). Sequences belonging to FERRY containing species were extracted and aligned using MAFFT with default settings.[56] Each alignment was trimmed using trimAL.[57] The maximum likelihood (ML) tree was estimated using IQTree[58] whereby each protein was represented as a partition.[59] The Whelan and Goldman matrix[60] with ML optimized amino acid frequencies (WAG+FO) was used as common model for all partitions. Branch support was calculated by IQTree via ultra-fast bootstrapping (UFBoot, 10,000).[61] The consensus tree with the presents/absence information was visualized using the R package ggtree (Version 2.0.4).[62,63]

FERRY evolution and ancestral state reconstruction

The identified orthologous genes were used to estimate the ancestral composition of the FERRY complex. The probability for each protein's presence at each internal node was estimated using Pagel's algorithm[64] implemented in the R package ape (Version 5.3).[65]

Antibody production

Rabbit polyclonal antibodies against Fy-4 were raised in NZW rabbits using standard procedures. 200 μg of recombinant protein emulsified in Complete Freund's adjuvant was used for immunization. Three boosts were done at 4-week intervals using 200 μg of recombinant protein emulsified in Incomplete Freund's adjuvant. The final bleed was harvested 10 days after the last boost. Antibodies were affinity-purified on Fy-4 immobilized on a HiTrap NHS-activated HP column (GE Healthcare). Antibodies were eluted using Pierce Gentle Ag/Ab Elution Buffer (ThermoFisher).

Mouse monoclonal antibodies against different components of the FERRY complex were raised in Balb/c mice after subtractive immunization[66] with Fy-5. Mice were injected with recombinant Fy-5 in the presence of the immunosuppression drug cyclophosphamide in order to preferentially eliminate Fy-5-reactive B and T lymphocytes. Thereafter the mice were immunized with the entire FERRY complex. Hybridoma were generated using PEG fusions following standard protocols. Clones reacting with individual components of the FERRY complex were selected in a multiplex electrochemiluminescence assay on the MSD platform (Mesoscale Discovery, Rockville, MD). Antibodies were purified from hybridoma supernatant using HiTrap Protein G columns (GE Healthcare).

Antibody validation

Validation of in-house produced antibodies against components of the FERRY complex for Western blot (WB) were tested against 100 ng, 10 ng and 1 ng of recombinant FERRY complex. Candidates with high sensitivity (detection of 1 ng) and good selectivity (preferably no or no interfering additional signal) were chosen.

Immunofluorescence (IF) validation of the Fy-2 and Fy-4 antibodies raised for this study for was performed using the respective FERRY component KO cell lines (Figure S1F). We subsequently compared the fluorescence signal in wildtype and the KO cell line. For Fy-2 we observed a strong reduction of fluorescence signal in *fy-2* Ko cell line, while the fluorescence of Rabankyrin-5 seems unchanged (Figure S1C, upper panels). Although the WB indicates the disappearance of the Fy-2, we cannot rule out that that there is a small fraction of Fy-2 left. We also tried to generate a KO using a full locus deletion of fy-2, which had a lethal effect on HeLa cells. Thus, we did not obtain any clones. The fluorescence signal for Fy-4 almost completely disappeared in the *fy-4* Ko cell line, while again the Rabankyrin-5 signal seems unchanged (Figure S1C, lower panels).

Antibodies

The following primary antibodies were used for IF or WB experiments at the concentrations or dilutions indicated: anti-EEA1 (rabbit, polyclonal, laboratory-made, IF 1:1000), anti-Rabankyrin-5 (rat, monoclonal, laboratory-made, IF 1:2000), anti-Map2 (rabbit, polyclonal, Chemicon, IF 1:1000), anti-pNF-H (mouse, monoclonal, Biolegend, IF 1:5000), anti-Fy-1 (rabbit, polyclonal, Sigma Aldrich, HPA039951, WB 1:1000) anti-Fy-2 (mouse, monoclonal, laboratory-made, IF 1:1000, WB 0.5 μg/μL), anti-Fy-3 (rabbit, polyclonal, Sigma Aldrich, HPA037871, WB 1:1000), anti-Fy-4 (rabbit, polyclonal, laboratory-made, IF 1:1000, WB 0.5 μg/μL), anti-Fy-5 (mouse, monoclonal, laboratory-made) WB (0.5 μg/μL), anti-GAPDH (rabbit, monoclonal, Sigma Aldrich, G8795, WB 1:5000), anti-TNS1 (rabbit, polyclonal, Atlas Antibodies WB 1:1000), anti-AK4 (rabbit, polyclonal, Atlas Antibodies, WB 1:1000), anti-PHKA1 (rabbit, polyclonal, Atlas Antibodies, WB 1:1000), anti-Alcam (rabbit, polyclonal, WB 1:1000), anti-BACE2 (rabbit, polyclonal, Atlas Antibodies, WB 1:1000), anti-MDH2 (rabbit, polyclonal, Atlas Antibodies WB 1:500), anti-MRPL41 (rabbit, polyclonal, Atlas Antibodies WB 1:1000), anti-Flag (mouse, monoclonal, Sigma Aldrich, WB 1:10000 or 1:7500), anti-RPL3 (rabbit, polyclonal, Proteintech, WB 1:2000) and anti-RPS3a (rabbit, polyclonal, Proteintech, WB 1:2000).

The following fluorescent secondary antibodies for immunostainings were purchased from Invitrogen and used in a 1:1000 dilution: Goat anti-Rat IgG (H + L) Highly Cross-Adsorbed Secondary Antibody, Alexa Fluor 488, Goat anti-Mouse IgG (H + L) Highly Cross-Adsorbed Secondary Antibody, Alexa Fluor 568, Goat anti-Mouse IgG (H + L) Cross-Adsorbed Secondary Antibody, Alexa Fluor 405, Goat anti-Rabbit IgG (H + L) Cross-Adsorbed Secondary Antibody, Alexa Fluor 647, F(ab')2-Goat anti-Rabbit IgG (H + L) Cross-Adsorbed Secondary Antibody, Alexa Fluor 647, Goat anti-Mouse IgG (H + L) Cross-Adsorbed Secondary Antibody, Alexa Fluor 488. For WB horseradish peroxidase (HRP) secondary antibodies were supplied from Jackson ImmunoResearch and used at a 1:10 000 dilution.

HEK 293 lysate preparation

FreeStyle 293-F Cells (Thermo Fisher Scientific) were grown in suspension culture in FreeStyle 293 Expression Medium (Thermo Fisher Scientific) to a density of 4 x 10^6 cells/ml and harvested by centrifugation (500 x g, 10 min, 20°C). The cell pellets were suspended in lysate buffer (6 mL/L cell culture, 50 mM HEPES (pH 7.5), 100 mM NaCl, 5 mM $MgCl_2$, 1 mM DTT, 0.1% Tween 20), supplemented with a protease inhibitor cocktail and immediately flash frozen in liquid nitrogen. For lysate preparation the pellets were melted, lysed using a microfluidizer (LM20, microfluidics). The lysate was subsequently clarified by a two-step centrifugation (4000 rpm/1935 x g, 10 min, 4°C and 22 500 rpm/61 236 x *g*, 25 min, 4°C), yielding around 15 mL cells lysate per liter cell culture.

GST-FERRY interactor screens

The GST-FERRY interactor screen was performed at 4°C in gravity flow filter columns (Poly-Prep Chromatography Column, Bio-Rad). 500 μL Glutathione Sepharose 4B (GE Healthcare) was added to 0.8 μmol of GST or 7 mg of GST-FERRY complex in 9 mL SEC buffer and incubated for 2.5 h on a rotating wheel. The solution was let run through and the resulting bed of beads was washed 3 × 2 mL SEC buffer. 10 mL of freshly prepared HEK 293 lysate was added to each column and incubated for 1.5 h on a rotating wheel. The lysate was allowed to flow through and another 5 mL of cell lysate was added to each column and also run through the column. The columns were extensively washed with 4 mL lysis buffer and 2 × 5 mL and 2 × 7 mL SEC+ buffer (20 mM HEPES, pH 7.5, 250 mM NaCl, 20 mM KCl, 20 mM $MgCl_2$, 1 mM DTT and 0.1% Tween 20). For the elution of the proteins the columns were incubated with 500 μL of GSH buffer for 40 min on a rotating wheel. The elution fractions were visualized by SDS PAGE and further analyzed by mass spectrometry.

To isolate FERRY-associated RNA, from a HEK 293 lysate the GST-FERRY interactor experiment was performed as described with slight modifications. For the elution of the proteins and the associated RNA, RLT buffer from the AllPrep DNA/RNA/miRNA Universal Kit (Qiagen) was supplemented with 1% β-Mercaptoethanol and 20 mM GSH and the pH adjusted to 7.5. The subsequent isolation of nucleic acids was performed using the AllPrep DNA/RNA/miRNA Universal Kit (Qiagen) according to the manufacturer's protocol. The obtained RNA samples were flash frozen and stored at −80°C. Prior sequencing, the concentration of the samples was determined by spectrophotometer (NanoDrop Lite, Thermo Scientific) and the samples were analyzed using a 2100 Bioanalyzer (Agilent).

Mass spectrometry

Samples were separated on SDS PAGE, visualized with Coomassie staining and entire gel lanes cut in 10 pieces each of which was processed individually. Proteins were in-gel reduced by dithiothreitol (DTT), alkylated by iodoacetamide and digested overnight with trypsin (Promega). The resulting peptide mixtures were extracted twice by exchange of 5% formic acid (FA) and acetonitrile, extracts pulled together and dried in a vacuum centrifuge. Peptides were resuspended in 25μL of 5% FA and 5μL aliquot was analyzed by LC-MS/MS on a nanoUPLC system interfaced on-line to a Q Exactive HF Orbitrap mass spectrometer (both Thermo Fischer Scientific). The nanoUPLC was equipped with an Acclaim PepMap100C18 75 μm i.d. x 20 mm trap column and 75 μm × 50 cm analytical column (3μm/100A, Thermo Fisher Scientific). Peptides were separated using a 80 min linear gradient; solvent A - 0.1% aqueous FA, solvent B - 0.1% FA in acetonitrile. Blank runs were introduced after each sample analysis to minimize carryover. Instrument performance was monitored with QCloud system.[67] Data were acquired using a Top 20 approach; precursor *m/z* range was 350–1600 and dynamic exclusion time was 20 s. The lock-mass function was set on the background ion (Si(CH3)2O)6 at *m/z* 445.12. Acquired spectra were converted into the.mgf format and merged into a single file for each sample.

Acquired data were processed with the MaxQuant software package (v.1.6.10.43[68]) using default setting iBAC options, with Match-Between-Runs (MBR) disabled. Enzyme specificity was trypsin, number of allowed miscleavages – two; variable modification – cysteine carbamidomethyl, propionamide; methionine oxidation; protein N terminus acetylated.

Mass photometry

Mass Photometry (MP, iSCAMS) of the FERRY complex was performed on a One^{MP} instrument (Refeyn, Oxford, UK) at room temperature. High precision 24 × 50 mm coverslips (Thorlabs CG15KH) were cleaned with ultrasound, rinsed with isopropanol and water and dried with clean nitrogen gas.[69] 20 μL diluted FERRY complex (43 and 34 nM, in PBS) was spotted into a reusable culture well gasket with 3 mm diameter and 1mm depth (Grace Bio-Labs). MP signals were recorded for 60 s at a suitable concentration in order to detect a sufficient set of target particles (>500). Raw MP data were processed in the DiscoverMP software (Refeyn, Oxford, UK).

Sucrose density gradient centrifugation to analyze ribosome association

Expression of 2xFlag-Pre-Scission protease cleavage site-His_6-Fy2 was induced in stably transfected HEK 293 cells by addition of 1 μg/μL tetracycline for 24 h. Cells were treated with 100 μg/mL cycloheximide for 10 min prior to harvesting. Cells were resuspended in Lysis Buffer (20 mM HEPES pH 7.6, 100 mM KCl, 5 mM $MgCl_2$, 0.5% NP-40, 100 μg/mL cycloheximide, 2 mM DTT, 0.625% Triton X-100, 0.625% deoxycholate supplemented with protease and RNase inhibitors) and lysed on ice for 5 min. Cell debris were pelleted by centrifugation at 10,000 g for 10 min at 4°C. Extracts were separated on 10–50% sucrose gradients prepared in Lysis Buffer lacking detergents by centrifugation in an SW-40Ti rotor at 35,000 rpm for 2.5 h.[70] Gradients were fractionated and an absorbance profile at 260 nm generated using a BioComp Gradient Master.[71] Relevant fractions were pooled and proteins precipitated using 20% trichloroacetic acid. Proteins were separated by SDS-PAGE and analyzed by WB using anti-Flag (Sigma-Aldrich F3165; 1:7500), anti-RPL3 (Proteintech 11005-1-AP; 1:2000) and anti-RPS3a (Proteintech 14123-1-AP; 1:2000) antibodies.

Library preparation and sequencing

mRNA was enriched from 100ng DNase treated total RNA using the NEBNext rRNA depletion Kit (human, mouse, rat, NEB) according to the manufacturer's instructions. Final elution was done in 5 μL nuclease free water. Samples were then directly subjected to the workflow for strand specific RNA-seq library preparation (NEBNext Ultra II Directional RNA Library Prep, NEB). 0.15 μM NEB Adaptor were used for ligation. Non-ligated adaptors were removed by adding XP beads (Beckmann Coulter) in a ratio of 1:0.9. Dual indexing (GST-FERRY association screen) or unique dual indexing (RNASeq of FERRY component KO cell lines) was done during the following

PCR enrichment (12 cycles, 65°C)). After two more XP bead purifications (1:0.9) libraries were quantified using the Fragment Analyzer (Agilent). Libraries were equimolarly pooled before sequencing them with a length of 75 bp in single end mode on an Illumina NextSeq 500 system to a depth of at least 2 x 10^7 reads (GST-FERRY association screen) or with a length of 2 x 150 bp in paired end mode on an Illumina NovaSeq 600 system to a depth of at least 5 x 10^7 read pairs (RNASeq of FERRY component KO cell lines).

Rab5 affinity chromatography

GST-Rab5 affinity chromatography was carried out as described before.[26] In summary, GST-Rab5:GDP or GST-Rab5:GTPγS loaded glutathione Sepharose was incubated with bovine brain cytosol, the beads extensively washed and the bound proteins subsequently eluted. The resulting mixture of Rab5 effector proteins was further purified by SEC and anion exchange chromatography. Fractions were analyzed using silver stained SDS PAGE.

In vitro translation binding assay

Binding assays with *in vitro* translated proteins were essentially performed as described.[72] Briefly, [^{35}S]-methionine-labelled proteins were transcribed and translated using a TnT coupled transcription–translation kit (Promega) according to the manufacturer's protocol. Resulting proteins were incubated with GST-Rab5:GDP or GST-Rab5:GTPγS loaded Glutathione Sepharose for 2 h at 4°C. Subsequently, the beads were washed and Rab5-bound proteins were eluted and analyzed by SDS PAGE and fluorography as described.[26]

mRNA production and electrophoretic motility shift assays

mRNA sequences for *mrpl41*, *mdh2*, *uchl1*, *atp5f1b*, *gstp1*, *prdx5*, *cox6b*, *cox8a* and *pigl* comprise the coding region, the 3′ and 5′ untranslated regions (UTRs) and an additional polyA appendix of 50 adenines (Table S3). The mRNAs were produced by *in vitro* transcription using the T7 RiboMAX Express Large Scale RNA Production System (Promega) according to the manufacturer's protocol. Resulting RNA was purified using a Phenol:Chloro-form extraction and an isopropanol precipitation as described in the manual of the mMESSAGE mMACHINE T7 Transcription kit (Thermo Fisher). In brief, the *in vitro* transcription reactions were quenched with Ammonium acetate stop solution from the mMESSAGE mMACHINE T7 Transcription Kit (Thermo Fisher) and supplemented with Phenol:Chloro-form:Isoamyl Alcohol 25:24:1 (Sigma Aldrich). The aqueous phase was recovered and RNA precipitated by adding equal amounts of isopropanol. After chilling at - 20°C for at least 15 min, the precipitated RNA was pelleted by centrifugation (20 800 x g, 15 min, 4°C), the supernatant removed and the pellet resuspended in RNAse-free water. RNA concentrations were determined by spectrophotometer (NanoDrop Lite, Thermo Scientific)' and the RNA was stored at - 80°C until usage.

For direct protein-RNA interaction assays, 10 pmol of FERRY complex (500 nM) was mixed with *in vitro* transcribed mRNA (10 nM to 1μM) in varying protein/RNA ratios in SEC buffer in a total volume of 20 μL and incubated for 80 min at 37°C. The samples were analyzed using gel electrophoresis with 1% agarose gels. Gels were always run as duplicates and one gel stained for RNA using SYBR Gold Nucleic Acid Gel Stain (Invitrogen) the other stained for proteins with SYPRO Red Protein Gel Stain (Sigma Aldrich). Both dyes were used according to the manufacturers' protocols.

Direct protein-RNA interaction assays in presence of Rab5:GTPγS were performed, with 15 pmol of *mrpl41* mRNA (430 nM) mixed with 15 pmol FERRY complex (430 nM) and varying amounts of Rab5:GTPγS (from 430 nM to 4.3 μM) as indicated in Figure 3C in SEC buffer in a total volume of 35 μL. The mixture was incubated for 80 min at 37°C and the samples were analyzed by ethidium bromide-stained gel electrophoresis using 1% agarose gels.

RNA immunoprecipitation after UV crosslinking

Stably transfected HEK 293 cell lines for the tetracycline inducible expression of 2xFlag-Pre-Scission protease cleavage site-His6-Fy2, Fy2-His6-Pre-Scission protease cleavage site-2xFlag or the tag alone were generated using the HEK 293 Flp-In T-REx system (ThermoFischer Scientific). Expression of the transgenes was induced by addition of 1 μg/μL tetracycline for 24 h, and cells were grown in the presence of 100 μM 4-thiouridine for 9 h before crosslinking with 360 mJ/cm^2 irradiation at 365 nm.[73–75] Cells were harvested, resuspended in a buffer containing 50 mM Tris-HCl pH 7.8, 150 mM NaCl, 1.5 mM MgCl2, 0.1% NP40, 5 mM β-mercaptoethanol, cOmplete-EDTA-free protease inhibitors and lysed by sonication. RNA-protein complexes were retrieved from the cleared lysate on anti-Flag M2 beads (Sigma Aldrich) and eluted using 3x Flag peptide. Co-purified RNAs were subjected to partial RNase digestions using RNace-It (Agilent Technologies) and complexes were immobilized on Ni-NTA under denaturing conditions (50 mM Tris-HCl pH 7.8, 300 mM NaCl, 10 mM imidazole 6 M guanidium-HCl, 0.1% NP40, 5 mM β-mercaptoethanol). Alkaline phosphatase treatment was performed before labeling of the RNA fragment 5′ ends with [^{32}P] using T4 PNK. Complexes were eluted from the Ni-NTA using imidazole and precipitated with 20% trichloroacetic acid before separation by denaturing polyacrylamide gel electrophoresis and transfer to a nitrocellulose membrane. Labeled RNAs in the eluate were then detected by autoradiography and proteins were subjected to WB using an anti-Flag antibody (Sigma-Aldrich F3165; 1:10000).

Generation of HeLa KO cell lines

Generation of KO cell lines by induced random mutations

To generate gene knockouts in HeLa, we used CRISPR/Cas9 cleavage induced random (NHEJ mediated) mutations using guide RNAs targeted 5′ end of the coding sequence of the genes of interest. We used electroporation of Cas9 protein complexed with

crRNA and trRNAs (altR, IDT), using the Neon electroporator device and kits (Invitrogen) with concentrations and electroporation settings as previously described.[76] For list of crRNA protospacers used for each gene, see Table S3. The success of the gene disruption was initially assessed by Western blot of single cell derived clones. The disruption of the target alleles was further confirmed by fluorescent PCR and Sanger sequencing of PCR amplicons (For the genotyping primers used and description of the alleles, see Table S3.

Generation of a fy-2 KO in HeLa cells by critical exon deletion

In order to generate a *fy-2* knockout in HeLa cells, we deleted exon 6 to 7 (deletion of ca. 1340 bp). Deletion of these two exons generates an out-of-frame transcript with a premature stop codon which leads to a truncated protein of 187 aa.

Guide RNAs specific to the *fy-2* locus were selected based on low off-target activity using http://crispor.tefor.net. The guide RNAs were ordered as crRNA from Integrated DNA Technologies (IDT).

HeLa cells were transfected with Cas9 protein (IDT Cat.no. 1081061) complexed with crRNA (IDT, Alt-R) and tracrRNA (IDT Cat.no. 1072534) using the Neon electroporator device and kits (Invitrogen) with concentrations and electroporation settings as previously described.[76] For a list of crRNA protospacers used for each condition, see Table S3. 72 h post-transfection cells were single-cell sorted into 96-well plates. Cell sorting was performed in a BD FACSAria Fusion flow cytometer (Beckton Dickinson). Single-cell clones were genotyped by PCR. Briefly, genomic DNA was extracted using the QuickExtract DNA extraction kit (Epicentre) following the manufacturer's instructions. PCR was performed using Phusion Flash High-Fidelity PCR Master Mix (ThermoFisher) with gene-specific primers. Amplicons of the deleted alleles were verified by Sanger Sequencing. For the genotyping primers used and description of the alleles, see Table S3.

RNA extraction from HeLa cells

RNA was isolated from 1 to 2 million adherent grown HeLa cells. After detachment cells were pelleted by centrifugation (2000 x g, 5 min, 4°C) and the supernatant removed. The pellet washed twice with 500 μL PBS and subsequently homogenized in 1 mL Trizol and the cells lyzed by repeated pipetting until all cell clumps disappeared. After addition of 200 μL Chloro-form the samples were shaken vigorously for 15s and incubated for 3 min at rt and centrifuged (11 000 rpm/12 000 x g, 15 min, 4°C) to allow for phase separation. The RNA containing aqueous phase was collected and further purified using the RNeasy MinElute Cleanup Kit (Qiagen) according to the manufacturer's protocol. In brief, the samples were supplemented with 350 μL RLT buffer, mixed and further supplemented with 250 μL of ethanol and again mixed by pipetting. The sample was transferred into spin column and centrifuged with (11 000 rpm/12 000 x g, 1 min, 4°C). The samples were washed once with 500 μL 80% ethanol and eluted in 30 μL nuclease-free water. The obtained RNA samples were flash frozen and stored at −80°C. Prior sequencing, the concentration of the samples was determined by spectrophotometer (NanoDrop Lite, Thermo Scientific) and the samples were analyzed using a 2100 Bioanalyzer (Agilent).

Single molecule fluorescence *in situ* hybridization and immunostaining

Endosomes and endogenous mRNAs were stained by using the ViewRNA Cell Plus Assay kit (Invitrogen, 88–19000). The kit consists of 16 solutions that are used to perform an immunofluorescence staining followed by a single molecule fluorescence *in situ* hybridization (smFISH) using the sequential branched-DNA amplification technique. The manufactures protocol for 96 well plates was adapted to a 384 well plate format by down-scaling to 12.5 μL/well for steps containing staining solutions and to 25 μL/well for steps containing washing/fixing solutions (96 well protocol: 50 μL and 100 μL, respectively). For details see the manufactures protocol (https://assets.thermofisher.com/TFS-Assets/LSG/manuals/88-19000.pdf).

In brief, all steps were performed manually using an 8-channel aspirator for removal and automated multi-channel pipettes for addition of liquids. All wash steps following fixation and immunostaining were done 3 times with PBS including RNase inhibitor solution, whereas all wash steps following smFISH were done 5 times with RNA wash buffer solution. Cells were fixed and permeabilized using the provided solutions of the kit. After washing with PBS, cells were incubated with blocking buffer, primary antibody solution (including EEA1 and Fy-2 antibodies at a dilution of 1:2000 and 1:1000, respectively) and secondary solutions (including antibodies against rabbit and mouse IgG labeled with Alexa 488 or Alexa 568 (Alexa 647 for probe HPRT1), respectively, at a dilution of 1:500). After immunostaining cells were fixed and ready for smFISH. Different probes were used to label different mRNAs (Invitrogen, all probes were of type 6 (647nm), except the house-keeping gene HPRT1 (type 1, 546nm); *atp5f1b*: VA6-3168504, *gla*: VA6-3168560, *gstp1*: VA6-3169160, *cox6b*: VA6-3171299, *cox8a*: VA6-3171305, *mdh2*: VA6-3172506, *mrpl41*: VA6-3169863, *mrps35*: VA6-3179781, *psma1*: VA6-3173135, *polyA*: VF6-12675, *rims1*: VA6-3176214 and *hprt1*: VA1-11124). Cells were incubated for 2h at 40°C with a diluted probe. After washing the cells with RNA wash buffer solution, the protocol was continued the next day with the smFISH branched-DNA amplification technique steps. Subsequently, cells were incubated with pre-amplifier, amplifier and label solution each for 1h at 40°C. Finally, the cells were stored in PBS containing DAPI (1 μg/ml) to stain the nuclei and CellMaskBlue (CMB) (0.25 μg/ml) to stain the cytoplasm.

Preparation of hippocampal cultures

Primary rat hippocampal neurons used in this study were obtained and cultured in two different ways. For initial Fy-2 localization experiments, the protocol for culturing hippocampal neurons was adapted from[20] with slight modifications. In brief, neurons were isolated from rat embryos at E17. The rat hippocampi from embryos of either sex were dissected in PBS (25 mM Na-phosphate buffer, pH 7.4, 110 mM NaCl, 1 mM EDTA) and dissociated in digestion solution (100 mg/mL DNAse I and 200 Units Papain in PBS) for 20 min. After two washes of the tissue with plating medium (DMEM containing 10% FCS, 2 mM glutamine, 50 mg/mL penicillin/

streptomycin, Invitrogen), it was triturated in plating medium and subsequently cells counted. The neurons were plated on glass cover slips coated with 1 mg/mL poly-L-lysine (Sigma-Aldrich) at a density of 25 000 cells/ml in the presence of a mouse astrocyte feeder layer, derived from the mouse cortex from mice of age P0-P3 of either sex.[77]

Primary neurons for mRNA localization experiments were obtained and cultured according to the following protocol. Neuronal cultures were prepared from dissociated hippocampi of P0/P1 SD rats as previously described.[12] Hippocampi were collected in Dissociation Medium on ice (DM with 1 mM HEPES, 82 mM Na_2SO_4, 30 mM K_2SO_4, 5.8 mM $MgCl_2$, 0.252 mM $CaCl_2$, 20 mM Glucose, 0.001% Phenol Red) and treated with cysteine-activated papain solution in DM (10 mL DM, 3.2 mg Cysteine, 300 μL Papain Sigma P3125, pH readjusted to 7, filtered sterile) two times 15 min at 37°C before several washes with cold DM and Neuronal growth medium (NGM: Neurobasal A supplemented with B27 and Glutamax). Dissociation of the tissue was achieved by trituration through a 10 mL pipette for 10 times. Before counting in a Neubauer chamber, cells were pelleted by centrifugation for 5 min, 67 x g at 4°C, resuspended in cold NGM and 30 000 cells were seeded in 250 μL NGM on poly-D-Lys coated 14 mm MatTek glass bottom dishes. After attachment of the cells (2–3 h later) 0.7 mL conditioned NGM (80% NGM, 15% glia-conditioned NGM, 5% cortical neuron-conditioned NGM) was added and regular feeding by addition of NGM was performed thereafter. The neurons were kept in an incubator at 37°C in a humidified atmosphere with 5% CO_2.

Immunostaining of neurons

Immunostaining was performed at room temperature and the plates were subsequently stored at 4°C if necessary. After adhesion, cells were washed once with PBS and fixed using 3% Paraformaldehyde (PFA) for 15 min. After washing with PBS, residual PFA was quenched using 500 mM Ammonium chloride in PBS for 10 min and the cells were washed 3 times with PBS. For permeabilization the cells were treated with 0.1% Triton X-100 in PBS for 3 min and subsequently washed three times with PBS. After blocking with 10% FBS for 20 min, the cells were incubated with the primary antibody for 2 h. Before and after the application of the secondary antibody for 1 h, the cells were washed 3 times with PBS.

High sensitivity FISH and immunostaining in neurons

In situ hybridization was performed using the ViewRNA ISH Cell Assay Kit (Thermo Fisher) according to the manufacturer's protocol with the modifications described previously.[12] Probe sets targeting the respective mRNAs were purchased from Thermo Fisher. In brief, rat hippocampal neuron cultures grown for two weeks on MatTek glass bottom dishes were fixed for 20 min with PBS containing 1mM $MgCl_2$, 0.1 mM $CaCl_2$, 4% Sucrose and 4% PFA, pH 7.4 at room temperature, washed and subsequently permeabilized for 3 min with the provided detergent solution. Gene specific type1 (*uchl1*) and type6 (*mdh2*, *polyA*) probe sets were applied in 1:100 dilution for 3 h at 40°C. After several washes signal amplification steps with Pre-Amp/Amp and Label Probe reagents coupled to a 550 nm dye were all performed for 1 h at 40°C followed by washes at room temperature after each step. All probe sets and branched DNA reagents were diluted in the provided solutions 1:100. Immunostaining for Fy-2, endosome and mitochondria markers was performed after completion of the FISH protocol. FISH-stained cells were blocked for 30 min in blocking buffer (BB) at room temperature (BB: PBS with 4% goat serum) and incubated with primary antibodies in BB for 1 h at room temperature. After washing, secondary antibodies in BB were applied for 30 min, cells were washed and nuclei stained by a 3 min incubation with 1 μg/μL DAPI in PBS. Cells were washed in PBS and mounted with Aquapolymount (Polysciences).

Microscopy

Automated HeLa imaging

Confocal imaging was performed on an automated spinning disc confocal microscope (Yokogawa CV7000) using a 60×1.2NA objective. DAPI and CMB was acquired with a laser excitation at 405 nm and an emission band-pass filter BP445/45, Alexa 488 with a 488 nm laser and BP525/50 filter, Alexa 568 with a 561 nm laser and BP600/37 filter, Alexa 647 with a 640 nm laser and a BP676/29 filter. 9 fields were acquired per well as a stack with 4 z-planes and 1 μm distance. Each condition was done in duplicate wells and three independent experiments.

Spinning-disk neuron imaging

Neurons were imaged on a Nikon TiE spinning disk microscope equipped with a 100x/1.45NA Plan Apochromat, DIC oil immersion objective, Yokogawa CSU-×1 scan head and a Andor DU-897 back-illuminated CCD detector. Images were acquired with 600 ms exposure, while the laser intensities were adapted to the respective antibodies and requirements. Overview images of almost entire neurons were taken as a set of individual small images (6 x 6 images) with an overlap of 5% and combined using the Fiji[51] implemented Grid/Collection Stitching tool[78] without overlap computation.

Confocal neuron imaging

Images were acquired with a LSM780 confocal microscope (Zeiss) equipped with Zen10 software using a 63x/1.46-NA oil objective (alpha Plan Apochromat 63×/1.46 oil DIC M27) and Argon 488, DPSS 561 and HeNe 633 laser lines for excitation in single tracks and a MBS488/561/633 beam splitter. Images were acquired in 12-bit mode as z-stacks and a time series with 4x Zoom, 512px x 512 px resolution and 0.1 μm Tetraspec beads (ThermoFisher) imaged under the same conditions. The laser power and detector gain in each channel was set to cover the full dynamic range but avoid saturated pixels.

Western blotting

Cells were collected from a 10 cm cell culture dish, washed with cold PBS and subsequently lysed in PBS supplemented with 1% Triton X-100. HeLa cell lysates were clarified by centrifugation (14 000 rpm/20 800 x *g*, 15 min, 4°C) and the concentration determined using a BCA assay (Pierce BCA Protein Assay Kit, Thermo Scientific). After running an SDS PAGE (12%), the gel was subsequently transferred onto a nitrocellulose membrane (Amersham). Blots were washed with PBST (PBS supplemented with 0.1% Tween 20) and then incubated with WB blocking buffer (5% non-fat milk powder in PBST) over night at 4°C. After washing with PBST blots were then incubated with the primary antibodies (anti-Fy-1 to anti-Fy-5 and anti-GAPDH as a loading control) at the dilutions indicated earlier for 1 h at room temperature. After washing the secondary HRP antibody was applied to the blot for 1 h at room temperature. All antibodies were added in PBST with 5% milk. The blots were developed using ECL Western Blotting Reagents (Cytiva) on respective films (Amersham) in a Kodak X-OMAT 200 Processor.

QUANTIFICATION AND STATISTICAL ANALYSIS

Analysis of the mass spectrometry data

From the MaxQuant proteinGroups.txt file only protein groups with at least 1 unique peptide and which were identified in at least two out of three biological replicates in at least one condition were considered for differential abundance analysis using DEP v1.4.0.[79] After variance stabilizing normalization[80] of iBAQ intensities, missing values were imputed applying the nearest neighbor averaging imputation method (KNN) to missing at random (MAR) and left-censored imputation using a deterministic minimal value approach (MinDet) to missing not at random (MNAR) protein groups.[81] MNARs refer to those protein groups with missing values in all replicates of one of the two conditions while all other missing values are considered as MAR. The application of empirical Bayes statistics on protein group-wise linear models was done using limma[82] and differentially abundant proteins were identified by applying a log2 fold change threshold of 1 and an adjusted p value cutoff of 0.05.

Analysis of the RNA sequencing data

Raw reads were checked for their overall quality using FastQC v0.11.2.[83] For the sequencing data obtained from the HEK 293 lysate GST-FERRY interaction screen, read mapping to the human genome reference assembly (GRCh38_p13) and genes counts estimation based on Ensembl release v99[84] were done using STAR v2.5.2b (–outFilterMultimapNmax 1 –outSJfilterCountUniqueMin 8 3 3 3 –quantMode GeneCounts[85]; by taking read strandedness into account. For the sequencing data obtained from RNA extractions of wt HeLa and the FERRY subunit KO cell lines, read mapping to the human genome reference assembly (GRCh38_p10) and genes counts estimation based on Ensembl release v88[84] were done using STAR v2.7.3a (–outFilterMultimapNmax 1 –outSJfilterCountUniqueMin 3 1 1 1 –quantMode GeneCounts[85]; by taking read strandedness into account.

Count data were filtered for genes with more than 10 counts in any sample and served as input for differential gene expression analysis using DESeq2 v1.22.1.[86] An adjusted p value cutoff of 0.01 was applied to FDRs obtained by using IHW v1.10.1.[87] Results summary in form of an MA plot was done using ggplot2 v3.2.1[88] following layout settings from the ggpubr package v0.2.5.[89] A gene set enrichment analysis against the MSigDB C5 collection of ontology sets or hallmark gene sets (msigdbr v7.0.1[90]) was run using fgsea v1.8.0[91] excluding gene sets with less than 15 and more than 500 genes.[92] In addition, an enrichment analysis of gene ontology (GO) terms, kegg and reactome pathways was performed with the R-packages ClusterProfiler v3.10.1,[93] ReactomePA v1.26.0[94] and and BiomaRt v2.38.0.[95]

HeLa cell images

Microscopy images for the localization of Fy-2, EEA1 and different mRNAs in HeLa cells were processed using the stand-alone freely available software MotionTracking (MT) (http://motiontracking.mpi-cbg.de). Images of were imported into MT and subsequently corrected for the chromatic shift of individual channels based on images of Tetraspec beads. For quantification, fluorescent foci of EEA1 and mRNA were detected using automated object detection and the co-localization was calculated based on 0.35 overlap threshold.[48,96] Co-localization markers on endosomes with and without Bayesian correction for random co-localization was performed using MT as is described in.[48] Given that the reliability of the co-localization estimation is decreased in case of low numbers of mRNA puncta, images with less than 10 mRNA puncta per field of view were excluded from the co-localization analysis. The co-localization values of individual fields of view were averaged with a weighting by the number of RNA puncta.

Neuron images

Microscopy images for the localization of Fy-2, EEA1, mRNA and mitochondria in neurons were also processed with MT. Image sequences of fixed neurons were imported into MT and drift corrected and deconvoluted by algorithms implemented in MT. In a last step, images were corrected for the chromatic shift of individual channels based on images of Tetraspec beads before and after the imaging. Motion Tracking implemented object detection was used to determine the mRNA foci while subsequent image analysis and quantification was performed by visual inspection. Given the possible distance between the fluorescence signals of EEA1 and mRNA or Fy-2 and mRNA (Figure S4A), automated object detection followed by a co-localization analysis was not suitable for this purpose.

Multiple source localization microscopy

Samples were prepared in fresh STORM buffer as described in.[30] Image stack acquisition was performed with a Spinning Disc, Andor-Nikon TiE inverted stand microscope equipped with a spinning disc scan head (CSU-X1; Yokogawa), a fast piezo objective z-positioner (Physik Instrumente), a back-illuminated EMC CD camera (iXon EM + DU-897 BV; Andor), a Nikon Apo 100×1.45 Oil DIC objective and a OptoVar 1.5 lens (pixel size in x-y plane is 70.1nm). Samples were z-scanned for 2.5μm with 0.25μm steps. At each z-position for 3 channels (488, 561 and 647) 50 snap-shot images were acquired and 405 nm laser was used to re-activate fluorophores before moving to the next z-position. The multiple fluorophore localization was performed by algorithm described in[97] as it implemented in MT.